



Bachelor's Degree in Engineering for Industrial Technologies

Bachelor's project

Modelling of pumped storage hydropower with high-density
fluids

Author

Carlos López-Ibor Romero

Supervised by

Fabrizio Sossan

Madrid

Aug 2025

Declaration of Authorship

I hereby declare, under my own responsibility, that the Project presented with the title Modelling of pumped storage hydropower with high density fluid

at the ICAI School of Engineering of Comillas Pontifical University, during the academic year 2024–2025, is my own work, original and unpublished.


It has not been previously submitted for any other purpose. The Project is not a plagiarism of another work, either in whole or in part, and all information taken from other documents is properly referenced.

Signed: 
Carlos López-Ibor Romero

Date: 23.08.25

Authorized for submission of the project

THE PROJECT SUPERVISOR

Signed: 
Fabrizio Sossan

Date: 26.08.2025

Modelling of pumped storage hydropower with high density fluid

Author: López-Ibor Romero, Carlos.

Supervisor: Sossan, Fabrizio.

Collaborating Entity: ICAI – Universidad Pontificia Comillas

Project Abstract

This Bachelor's Thesis addresses the modeling of a pumped-storage hydropower plant using high-density fluids. The goal is to evaluate how replacing water with heavier fluids influences the generated power, the pressure distribution along the hydraulic circuit, and the overall efficiency of the plant. A one-dimensional (1D) modeling is used based on electrical analogies and state-space representation and different scenarios are simulated. Results show that fluids such as R-19 can deliver over 150% more power for the same infrastructure, without significant penalties in friction losses.

Keywords: Pumped-storage hydropower, one-dimensional modeling, high-density fluids, R-19, wave speed, hydraulic head, repowering.

Introduction

Pumped-storage hydropower plants are among the most important energy storage systems, as they provide flexible and dispatchable renewable electricity. Traditionally, water is used as the working fluid, but this project proposes the use of denser fluids as an alternative to enhance stored energy and turbine output without the need for additional civil works, just changing the fluid.

Project Definition

The main objective is to model in detail the hydraulic behavior of a pumped-storage plant when the working fluid density varies. The goals are: (1) to quantify the increase in turbine output when replacing water with fluids such as R-19, (2) to analyze changes in key variables such as wave speed, hydraulic head, and Reynolds number, and (3) to assess the feasibility of employing heavy fluids in closed systems without compromising efficiency or the HPP's safety.

Description of the Model

The study applies a one-dimensional (1D) model of the plant, where each hydraulic component is represented through electrical analogies (resistors, inductors,

capacitors). The penstock is discretized into segments governed by the continuity and momentum equations. Viscoelastic effects of the pipe wall are incorporated using the Kelvin–Voigt model. The final formulation is expressed in state-space, enabling efficient and flexible simulation.

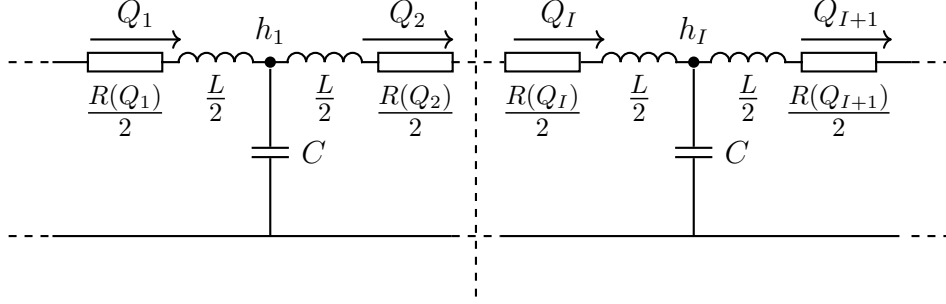


Figure 1: Schematic of the 1D discretized penstock model.

Results

The simulations confirm that denser fluids increase power output. For a gross head of 320 m and a flow rate of 50 m³/s, the turbine produces about 157 MW with water, compared to 392.4 MW with R-19. This 150% increase is consistent with the density ratio.

Moreover, the frictional head loss along the 1100 m penstock is nearly identical in both cases ($\approx 0.2\%$ of total head), showing that dense fluids do not result in additional losses. Also, it is interesting to see that the same pressure produced by a 320 m water column can be achieved with only 128 m of R-19 fluid, suggesting the potential for hydropower development in places with lower elevation differences.

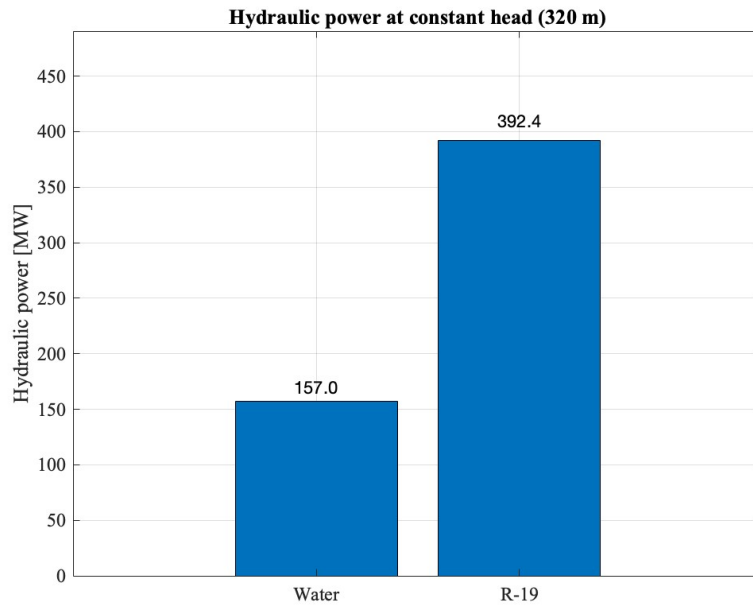


Figure 2: Turbine output power under 315 m head for Water vs. R-19 fluid.

References

1. Christophe Nicolet. *Hydroacoustic Modelling and Numerical Simulation of Unsteady Operation of Hydroelectric Systems*. Ph.D. Thesis, Thesis No. 3751, École Polytechnique Fédérale de Lausanne (EPFL), 2007. url: <https://infoscience.epfl.ch/record/97518>.
2. RheEnergise Ltd. *High-Density Hydro – A New Era for Energy Storage*. Accessed: 2025-06-16. 2022. url: <https://www.rheenergise.com/>.
3. Stefano Cassano. *Control and Scheduling of Hybrid Hydropower Plants with Batteries for Enhanced Flexibility in Future Power Systems*. Ph.D. Thesis, NNT: 2023UPSLM041. Mines Paris – PSL / Université Paris Sciences et Lettres, 2023. url: <https://pastel.hal.science/tel-04347682v1>.
4. RheEnergise Ltd. *Why We Use High-Density Fluids in Energy Storage – and How We Manage Safety*. Accessed: 2025-06-16. Discusses fluid containment and environmental safety measures. 2023. url: <https://www.rheenergise.com/technology/>.

Autor: **López-Ibor Romero, Carlos.**

Director: **Sossan, Fabrizio.**

Entidad Colaboradora: ICAI – Universidad Pontificia Comillas

Resumen del Proyecto

Este Proyecto Fin de Grado aborda la modelización de una central hidroeléctrica de bombeo utilizando fluidos de alta densidad. El objetivo es evaluar cómo la sustitución del agua por fluidos más pesados influye en la potencia generada, la distribución de presiones en el sistema hidráulico y la eficiencia global de la instalación. A través de un enfoque unidimensional (1D) basado en analogías eléctricas y representaciones en espacio de estados, se simulan diferentes escenarios, mostrando que fluidos como el R-19 permiten incrementos de potencia superiores al 150% para la misma infraestructura, sin penalizaciones significativas en pérdidas por fricción.

Palabras clave: Central hidroeléctrica de bombeo, modelado unidimensional, fluidos de alta densidad, R-19, velocidad de onda, cabeza hidráulica, repotenciación energética.

Introducción

Las centrales hidroeléctricas de bombeo representan uno de los sistemas de almacenamiento energético más relevantes, dada su capacidad de generar electricidad renovable de forma flexible y despachable. Tradicionalmente, emplean agua como fluido de trabajo, pero este proyecto plantea el uso de fluidos de mayor densidad como alternativa para aumentar la energía almacenada y mejorar la potencia de salida sin necesidad de grandes obras civiles adicionales.

Definición del Proyecto

El objetivo principal es modelar en detalle el comportamiento hidráulico de una central de bombeo sometida a variaciones en la densidad del fluido de trabajo. Se persigue: (1) cuantificar el aumento de potencia que puede lograrse al sustituir el agua por fluidos como el R-19, (2) analizar cómo cambian variables críticas como la velocidad de propagación de ondas, la cabeza hidráulica y el número de Reynolds, y (3) evaluar la viabilidad de emplear fluidos pesados en sistemas cerrados sin comprometer la eficiencia ni la seguridad.

Descripción del Modelo

El estudio emplea un modelo unidimensional (1D) de la planta, basado en analogías eléctricas que representan cada elemento hidráulico mediante resistencias, inductancias y capacitancias equivalentes. La tubería se discretiza en segmentos donde se aplican las ecuaciones de continuidad y cantidad de movimiento. Se incorporan además efectos viscoelásticos en las tuberías mediante el modelo de Kelvin–Voigt, con el fin de captar mayor precisión. La formulación final se expresa en espacio de estados, permitiendo una simulación eficiente y flexible.

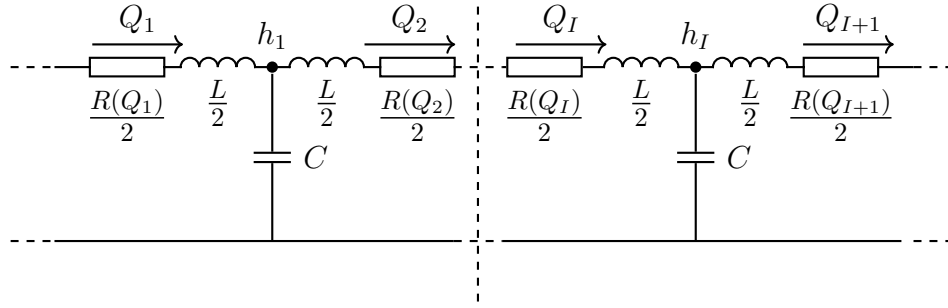


Figure 3: Esquema del modelo 1D de la tubería forzada discretizada en elementos equivalentes.

Resultados

Las simulaciones demuestran que el uso de fluidos de alta densidad aumentan notablemente la potencia de salida. Con una altura de 320 m y un caudal de 50 m³/s, la turbina genera aproximadamente 157 MW usando agua, frente a unos 392 MW con el fluido R-19. Esto supone un incremento cercano al 150%, en línea con la razón de densidades.

Asimismo, la caída de presión por fricción a lo largo de la tubería se mantiene prácticamente idéntica en ambos casos ($\approx 0,2\%$ del salto total), confirmando que el uso de fluidos densos no introduce pérdidas adicionales relevantes. Un resultado adicional es que la misma presión que produce 320 m de columna de agua se logra con tan solo 128 m de columna de R-19, lo que sugiere que este tipo de fluidos podrían habilitar instalaciones en lugares de menor desnivel.

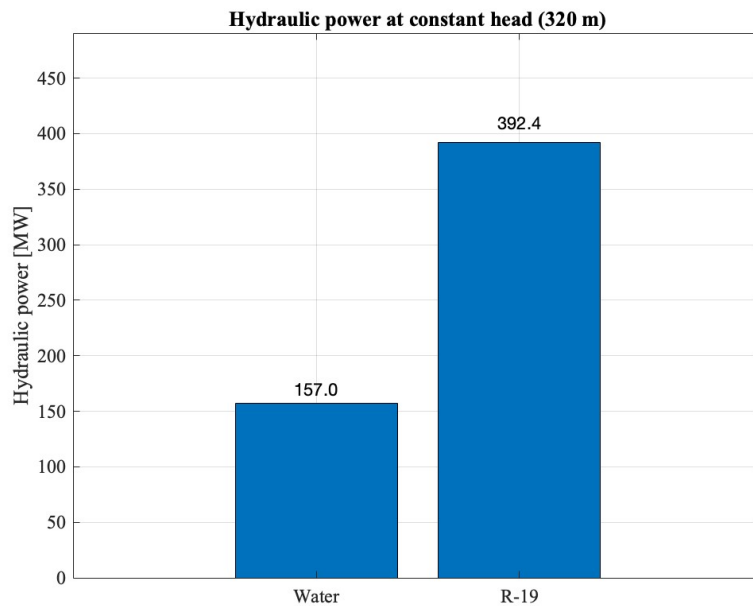


Figure 4: Potencia generada por la turbina bajo un salto de 315 m para agua y fluido R-19.

Referencias

1. Christophe Nicolet. *Hydroacoustic Modelling and Numerical Simulation of Unsteady Operation of Hydroelectric Systems*. Ph.D. Thesis, Thesis No. 3751, École Polytechnique Fédérale de Lausanne (EPFL), 2007. url: <https://infoscience.epfl.ch/record/97518>.
2. RheEnergise Ltd. *High-Density Hydro – A New Era for Energy Storage*. Accessed: 2025-06-16. 2022. url: <https://www.rheenergise.com/>.
3. Stefano Cassano. *Control and Scheduling of Hybrid Hydropower Plants with Batteries for Enhanced Flexibility in Future Power Systems*. Ph.D. Thesis, NNT: 2023UPSLM041. Mines Paris – PSL / Université Paris Sciences et Lettres, 2023. url: <https://pastel.hal.science/tel-04347682v1>.
4. RheEnergise Ltd. *Why We Use High-Density Fluids in Energy Storage – and How We Manage Safety*. Accessed: 2025-06-16. Discusses fluid containment

and environmental safety measures. 2023. url: <https://www.rheenergise.com/technology/>.

I would like to express my sincere gratitude to Dr. Fabrizio Sossan and Dr. Stefano Cassano for their invaluable supervision, guidance, and continuous support throughout the development of this work. I am deeply thankful for their trust in me, for proposing such an engaging and challenging topic, and for their constant availability to share knowledge, provide feedback, and offer encouragement at every stage of the project.

Contents

1	Motivation	1
1.1	Why Modeling is Essential in HPPs	1
1.2	Real-World Applications	1
1.3	Limitations of Experimental and Empirical Methods	2
2	Why 1D Models Are Preferred Over CFD	3
2.1	CFD: High-Fidelity Modeling	3
2.2	The Need for Speed: Operational Flexibility and Grid Dynamics . .	5
2.3	Advantages of 1D Modeling for HPP Simulation	6
2.4	Overview of the 1D Modeling Framework	6
3	1D Modeling of Hydraulic Elements in HPPs	9
3.1	Pipe (Penstock)	9
3.1.1	Governing PDEs: Continuity and Momentum Equations . .	9
3.1.2	Viscoelastic Effects in the Penstock	13
3.1.2.1	From Elastic to Viscoelastic Pipe Models	14
3.1.2.2	Kelvin–Voigt Model from Rheology to Hydraulics .	15
3.1.2.3	Numerical Form of the Viscoelastic Model	17
3.1.2.4	Impact on Wave Propagation and Damping	18
3.2	Valve	19
3.2.1	Modeling as Static or Dynamic Boundary Condition	19
3.3	Surge Tank	20
3.3.1	Capacitive and Resistive Behavior in the T-Branch	20
3.4	Turbines	22
3.4.1	Turbine Types	23
3.4.1.1	Francis Turbine	23
3.4.1.2	Pelton Turbine	23

3.4.1.3	Kaplan Turbine	24
4	State-Space Representation of the HPP System	25
4.1	From Discretized PDEs to State Equations	25
4.2	Building the System Matrix	26
4.3	Boundary Conditions and System Initialization	28
4.4	Coupling Hydraulic Elements	29
5	Fluid Density Considerations	35
5.1	Effect of Variable Density on System Behavior	35
5.2	Parameters that Need Adjustment	36
5.3	Candidate Fluids and Feasibility	36
6	Wave Speed in Hydraulic Transients	38
6.1	Introduction	38
6.2	Role of Wave Speed in Hydropower Modelling	38
6.3	Basic Wave Speed Formula	39
6.4	Corrected Formula and Pipe Support Coefficient	40
6.5	Assumptions and Limitations	41
6.6	Wave Speed in Different Pipe Materials	42
6.7	Comparison of Wave Speeds and Courant Numbers for Different Fluids	43
6.8	Conclusion	45
7	Hydraulic Head and Fluid Density	46
7.1	Definition and Physical Meaning of Hydraulic Head	46
7.2	Dependence of Head on Fluid Density	47
7.3	Recalculating Head for Non-Water Fluids	47
7.3.1	Example: Recomputing $h = 320$ m for Higher-Density Fluid	47
7.4	Implications for System Design and Control	48
7.5	Graphical Comparison of Head for Different Fluids	49
8	Friction Factor and Reynolds Number Analysis	50
8.1	Determining the Flow Regime	50
8.2	Friction Factor Models	51
8.3	Sensitivity to Friction Assumptions	53

8.3.1	Graphical Analysis of Density and Viscosity Effects on λ and Reynolds Number	54
9	Simulation Results and Comparative Analysis	59
9.1	Baseline Power Output with Water vs. R-19	60
9.2	Pressure (Head) Distribution Along the Penstock	60
9.3	Frictional Head Loss Distribution	62
9.4	Equivalent Head and Power for Different Fluids	63
9.5	Summary Table	63
9.6	Implications for Hydropower Repowering	66
	Bibliography	69

List of Figures

1	Schematic of the 1D discretized penstock model.	iv
2	Turbine output power under 315 m head for Water vs. R-19 fluid. .	v
3	Esquema del modelo 1D de la tubería forzada discretizada en elementos equivalentes.	vii
4	Potencia generada por la turbina bajo un salto de 315 m para agua y fluido R-19.	viii
2.1	Physical layout of a hydropower plant.	7
2.2	Equivalent electrical analog of the hydropower plant system.	7
3.1	Penstock of i elements	12
3.2	Single i -th segment	13
3.3	Schematic of the dual Kelvin–Voigt model used: two branches in parallel for pipe and fluid viscoelasticity.	14
3.4	Penstock of i elements	18
3.5	Regulated resistor coupling between h_I and h_{I+1}	20
3.6	Capacitor–resistor representation of the surge tank in the T-branch.	22
4.1	Valve between nodes h_1 and h_I	31
4.2	Surge tank in between nodes h_1 and h_I	33
6.1	Wave speed as a function of D/e ratio for different pipe materials. .	41
6.2	Wave speed comparison among materials.	43
6.3	Wave speed and Courant number comparison for Water, R-19, and Saturated Brine in a steel pipe.	44
7.1	Comparison of required head h for different fluids at constant pressure.	49
8.1	Values of Re_i per section and regime thresholds drawn.	54

8.2	Figures (a) and (b): Influence of flow rate and fluid properties on λ and Reynolds number.	55
8.3	Figures (a) and (b): Isolated effects of fluid properties and resulting head loss behavior.	57
9.1	Turbine mechanical power output at a fixed head of 320 m for Water vs. R-19. The higher-density fluid delivers substantially greater power from the same head and flow rate, reflecting the proportional increase of $\rho g H$ available energy.	61
9.2	Steady-state piezometric head profile along the penstock (1100 m length) at $Q = 50 \text{ m}^3/\text{s}$ for Water vs. R-19. The head at the reservoir is about 320 m and drops by only $\sim 0.6 \text{ m}$ due to friction by the turbine inlet.	62
9.3	Frictional head loss per 110 m pipe segment (10 segments total) for Water vs. R-19 at $Q = 50 \text{ m}^3/\text{s}$. Losses are uniformly low along the pipe, summing to about 0.64 m over the full length.	64
9.4	Total Frictional head loss for both fluids	64
9.5	Required static head to achieve the same pressure as a 320 m water column. R-19 (density 2500 kg/m^3) produces the same pressure in only about 128 m of head.	65

List of Tables

2.1	Hydraulic-to-electrical analogies in 1D modeling.	8
3.1	Comparison of common rheological models: Maxwell and Kelvin–Voigt.	13
3.2	Comparison of common hydraulic turbines	24
5.1	Comparison of Fluid Densities for Hydropower Use	37
6.1	Summary of ψ values for typical support conditions	40
6.2	Typical wave speeds for different pipe materials	42
8.1	Flow regime classification by Reynolds number	51
9.1	Main characteristics of the reference plant.	59
9.2	Physical properties of the working fluids.	60
9.3	Comparison of performance metrics for Water vs. high-density fluids at $Q = 50 \text{ m}^3/\text{s}$ and $H = 315 \text{ m}$. Turbine efficiency is 90% in all cases.	63

List of Parameters

Symbol	Description	Unit
A	Cross-sectional area of the pipe	m^2
A_{ref}	Reference cross-sectional area	m^2
A_{st}	Cross-sectional area of the surge tank	m^2
a	Wave propagation speed in fluid	m/s
a_0	Acoustic wave speed in rigid pipe	m/s
C	Hydraulic capacitance of a pipe segment	m^2
C_{fluid}	Capacitance from fluid compressibility	m^2
C_{n}	Courant number	—
C_{pipe}	Capacitance from pipe elasticity	m^2
C_{st}	Hydraulic capacitance of surge tank	m^2
C_{ve}	Equivalent viscoelastic capacitance	m^2
D	Internal pipe diameter	m
D_i	Diameter of pipe segment i	m
E	Young's modulus of the pipe material	Pa
E_{fluid}	Bulk modulus of the working fluid	Pa
E_{pipe}	Effective modulus for the pipe wall	Pa
E_{water}	Bulk modulus of water	Pa
e	Pipe wall thickness	m
g	Gravitational acceleration	m/s^2
H_{loss}	Head loss due to friction or geometry	m
H_v	Head drop across the valve	m
I	Number of discrete elements in the penstock	—

Symbol	Description	Unit
K	Bulk modulus of fluid	Pa
K_{st}	Local loss coefficient at surge tank	–
$K_v(s)$	Valve loss coefficient as a function of opening s	–
l	Total length of the penstock	m
L	Hydraulic inductance of a pipe segment	s^2/m^2
L_i	Length of pipe segment i	m
λ	Darcy–Weisbach friction factor	–
λ_i	Darcy–Weisbach friction factor for segment i	–
μ	Dynamic viscosity of the fluid	Pa·s
μ_{fluid}	Viscous damping coefficient of the fluid	Pa·s
μ_{pipe}	Viscous damping coefficient of the pipe wall	Pa·s
ν	Poisson’s ratio of the pipe material	–
P	General power (mechanical or hydraulic)	W
P_{hyd}	Hydraulic power extracted from fluid	W
P_{out}	Output mechanical power of the turbine	W
Q	Volumetric flow rate (discharge)	m^3/s
Q_c	Flow into or out of the surge tank	m^3/s
Q_f	Flow in fluid viscoelastic branch	m^3/s
Q_i	Flow entering segment i	m^3/s
Q_{i+1}	Flow exiting segment i	m^3/s
Q_p	Flow in pipe wall viscoelastic branch	m^3/s
$R(Q_i)$	Nonlinear resistance for flow Q_i	s/m^2
R_{fluid}	Hydraulic resistance of fluid branch	s/m^2
R_{pipe}	Hydraulic resistance of pipe wall branch	s/m^2
$R_{\text{st}}(Q)$	Nonlinear resistance at surge tank entry/exit	s/m^2

Symbol	Description	Unit
$R_v(s)$	Valve resistance dependent on opening s	s/m^2
R_{ve}	Equivalent viscoelastic resistance	s/m^2
s	Valve opening position (0 to 1)	–
t	Time	s
v	Flow velocity	m/s
V	Volume of fluid	m^3
V_0	Reference volume for strain definition	m^3
V_{st}	Volume stored in the surge tank	m^3
x	Axial position along the pipe	m
z	Elevation or vertical coordinate	m
ϵ	Pipe wall roughness height or strain	m or –
η	Turbine efficiency	–
ρ	Fluid density	kg/m^3
ρ_f	Density of the working fluid	kg/m^3
ρ_w	Density of water	kg/m^3
σ	Stress (mechanical)	Pa
ψ	Pipe support coefficient (anchoring effect)	–

Chapter 1

Motivation

1.1 Why Modeling is Essential in HPPs

Hydropower plants (HPPs) play a fundamental role in the world's energy mix due to their ability to produce renewable, dispatchable, and very efficient electricity supply. Due to their size and carefully planned operation in national grids, the operation, design, and safety of these plants require a thorough understanding of how water behaves through the hydraulic circuit.

Modeling is required since it allows researchers and engineers to model the dynamic responses of HPPs under varied operating conditions such as normal operation, transient operations such as valve closure, or emergency shut-down. These models are employed for design validation, performance optimization, failure prediction, and system control. Relying solely on experiment would be both economically and logistically impracticable without modeling, especially at the initial design stage or in the analysis of rare but significant circumstances such as water hammer or resonance effect.

In this context, accurate but computationally efficient modeling methods can save time and resources as well as contribute to safety and reliability.

1.2 Real-World Applications

Application of the models to real hydropower plants is widespread. They are used by engineers in penstocks and valve design so that it can withstand the transient load, size surge tanks or air chambers appropriately, and maintain turbine

performance within reasonable bands of efficiency for various flow conditions.

Operationally, real-time models may be employed for load forecasting and dispatch planning to model the rate at which a power plant reacts to changes in grid demand. They also allow for the integration of HPPs into hybrid renewable power systems, such as integrating with solar and wind, where hydro flexibility becomes a dominant advantage.

Aside from operations and design, models are also finding use in digital twins of HPPs for predictive maintenance, testing of virtual control strategies, and training of operators. These serve to underscore the real-world significance of sound and accurate modeling frameworks.

1.3 Limitations of Experimental and Empirical Methods

Experimental methods, though helpful, are hampered by the limitations of scale, cost, and practicability. It is not practical to build test-scale physical models of large hydraulic systems, especially for transient or emergency use. It is also not feasible to simulate actual plants under severe conditions without causing damage or interfering with operation.

Empirical methods based on historical data or truncated assumptions can offer quick insight but tend not to be universally applicable and miss higher-order interactions such as nonlinear wave transport, fluid-structure interaction, or density-dependent effects.

On the other hand, physics-based modeling, when validated versus available data, provides an organized way to extrapolate behavior, test what-if situations, and distill insight in situations where experiments or empirical approximations are infeasible. It offers a level of realism versus control that is critical in systems as sensitive and high-risk as HPPs.

Chapter 2

Why 1D Models Are Preferred Over CFD

2.1 CFD: High-Fidelity but Impractical for System-Level Modeling

Computational Fluid Dynamics (CFD) is the most accurate and rigorous approach for simulating general fluid systems, as it solves the *Navier–Stokes equations*, the fundamental partial differential equations governing fluid motion.

Governing Equations: Navier–Stokes

The behavior of incompressible fluid flow is described by the Navier–Stokes equations, which include:

Continuity Equation (Incompressible Flow)

$$\nabla \cdot \vec{V} = 0 \tag{2.1}$$

Momentum Equations

$$\rho \frac{D\vec{V}}{Dt} = -\nabla p + \rho \vec{g} + \mu \nabla^2 \vec{V} \tag{2.2}$$

Where:

- \vec{V} is the velocity vector,
- p is pressure,
- ρ is fluid density,
- \vec{g} is gravitational acceleration,
- μ is dynamic viscosity.

These equations are expressed in vector form. For more complex geometries such as pipe systems in HPPs, it is often necessary to express the equations in cylindrical coordinates.

Continuity Equation in Cylindrical Coordinates

$$\frac{1}{r} \frac{\partial}{\partial r}(ru_r) + \frac{1}{r} \frac{\partial}{\partial \theta}(u_\theta) + \frac{\partial u}{\partial x} = 0 \quad (2.3)$$

Momentum Equations in Cylindrical Coordinates

Radial (r) direction:

$$\rho \left(\frac{\partial u_r}{\partial t} + u_r \frac{\partial u_r}{\partial r} + \frac{u_\theta}{r} \frac{\partial u_r}{\partial \theta} + u \frac{\partial u_r}{\partial x} - \frac{u_\theta^2}{r} \right) = -\frac{\partial P}{\partial r} + \rho g_r + \mu \left(\nabla^2 u_r - \frac{u_r}{r^2} - \frac{2}{r^2} \frac{\partial u_\theta}{\partial \theta} \right) \quad (2.4)$$

Tangential (θ) direction:

$$\rho \left(\frac{\partial u_\theta}{\partial t} + u_r \frac{\partial u_\theta}{\partial r} + \frac{u_\theta}{r} \frac{\partial u_\theta}{\partial \theta} + u \frac{\partial u_\theta}{\partial x} + \frac{u_r u_\theta}{r} \right) = -\frac{1}{r} \frac{\partial P}{\partial \theta} + \rho g_\theta + \mu \left(\nabla^2 u_\theta - \frac{u_\theta}{r^2} + \frac{2}{r^2} \frac{\partial u_r}{\partial \theta} \right) \quad (2.5)$$

Axial (x) direction:

$$\rho \left(\frac{\partial u}{\partial t} + u_r \frac{\partial u}{\partial r} + \frac{u_\theta}{r} \frac{\partial u}{\partial \theta} + u \frac{\partial u}{\partial x} \right) = -\frac{\partial P}{\partial x} + \rho g_x + \mu (\nabla^2 u) \quad (2.6)$$

where:

- u is the velocity vector,
- p is pressure,

- ρ is density,
- ν is kinematic viscosity,
- g is body force (e.g., gravity).

These equations represent conservation of mass and momentum, capturing flow acceleration, convective terms, pressure gradients, viscous diffusion, and external forces. By numerically resolving them on a 3D grid, CFD provides detailed insight into local flow phenomena, such as turbulent eddies, pressure distributions, boundary layers, and cavitation patterns, making it ideal for component-level design.

However, this high fidelity comes at a steep computational cost. Solving Navier–Stokes for the full hydropower plant (HPP) piping and turbine geometry requires massive meshes and small time steps. Simulating just seconds of real operation can take hours or days on high-performance hardware. This makes CFD impractical for plant-scale or system-level modeling, especially when fast or near-real-time results are needed.

2.2 The Need for Speed: Operational Flexibility and Grid Dynamics

Hydropower plants must respond rapidly to grid frequency deviations, load changes, and emergency events. Examples include:

- **Frequency changes:** governors adjust wicket gates to balance grid frequency.
- **Water hammer:** rapid valve closures induce pressure surges.
- **Power outages:** abrupt flow stoppage triggers transient waves.

To analyze and control these events effectively, models must run faster than real time. CFD’s computational demands prevent iterative studies, controller tuning, and hardware-in-the-loop integration. We therefore require a faster, yet sufficiently accurate approach for system-level analysis.

2.3 Advantages of 1D Modeling for HPP Simulation

One-dimensional (1D) modeling simplifies spatial variability by averaging over cross-sections and capturing key dynamics via ordinary differential equations (ODEs). A common technique uses an *electrical analogy*, mapping hydraulic components to circuit elements.

This transforms complex PDEs into a network of R–L–C equations that run faster. Benefits include:

- **Speed:** Enables real-time or faster simulations for transients.
- **System-level fidelity:** Accurately captures surge pressure, flow dynamics, and oscillations.
- **Control integration:** Easily couples with turbine governors, electrical grids, and operational control blocks.

Though detail is sacrificed because three-dimensional effects are not resolved, the trade-off is acceptable for operational studies where overall plant behavior is of interest and speed is needed to be in sync with the grid or network.

2.4 Overview of the 1D Modeling Framework

A pertinent question arises at this stage: can a hydropower plant truly be represented using an electrical analogy?

The answer is affirmative. This approach, while abstract in nature, provides a coherent and mathematically robust simplification that enables system-level modeling with considerable computational efficiency. Figure 2.2 illustrates a comprehensive hydropower plant and its corresponding equivalent electrical circuit. In this transformation, each hydraulic component is mapped to an electrical counterpart, forming a network that preserves the essential dynamic behavior of the original system.

To construct this analog representation, each physical phenomenon within the hydraulic system is associated with a well-understood electrical component. The following correspondences are used:

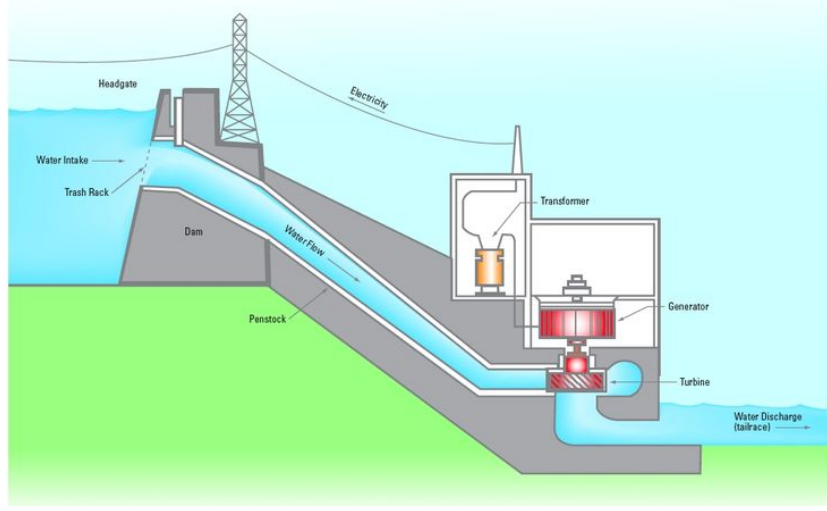


Figure 2.1: Physical layout of a hydropower plant.

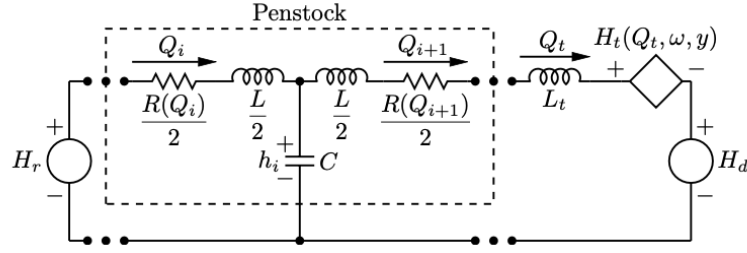


Figure 2.2: Equivalent electrical analog of the hydropower plant system.

- The volumetric flow rate (Q) is analogous to **electric current** (I), representing the time derivative of volume.
- The pressure head (H) corresponds to **voltage** (V), representing the potential difference that causes flow.
- Frictional losses, which dissipate energy, are modeled using resistors (R), where the pressure drop is proportional to flow.
- The inertia of the fluid mass, which resists changes in flow velocity, is represented by inductors (L), analogous to dynamic response.
- Elastic storage (e.g., due to pipe elasticity or surge tanks) is modeled by capacitors (C), which store and release energy based on pressure variations.

This analogy results in a element-segmented model comprising interconnected RLC components. Such a model can be simulated using established numerical methods for solving systems of ordinary differential equations. Moreover, its simplicity allows for seamless integration into real-time digital simulations, controller design environments, and large-scale system stability studies.

Hydraulic Component	Electrical Analog	Role
Flow rate Q	Current I	Volume per time, analogous to electric current.
Pressure head H	Voltage V	Driving force for flow.
Friction losses	Resistor R	Causes pressure drop, $V = I \cdot R$
Fluid inertia	Inductor L	Resists flow changes, $V = L \frac{dI}{dt}$
Elastic storage	Capacitor C	Stores pressure energy, $I = C \frac{dV}{dt}$

Table 2.1: Hydraulic-to-electrical analogies in 1D modeling.

In practical terms, upstream and downstream reservoirs are modeled as constant pressure sources (analogous to voltage sources or large capacitors), penstocks are discretized into cascades of RLC segments to capture pressure wave propagation, and surge tanks function as buffering capacitive elements. Turbines and control valves are typically represented by variable resistive elements that modulate flow according to system demands.

This modeling offers significant advantages in computational efficiency and integration potential, making it a powerful tool for the dynamic simulation and control-oriented analysis of hydropower plant systems.

Chapter 3

1D Modeling of Hydraulic Elements in HPPs

3.1 Pipe (Penstock)

3.1.1 Governing PDEs: Continuity and Momentum Equations

The behavior of the water inside the penstock can be described using the 1D equations of mass and momentum conservation. Under standard assumptions of incompressible flow, the system of partial differential equations (PDEs) governing the flow and pressure dynamics for a control volume dx is as follows [1]

$$\begin{cases} \frac{\partial h}{\partial x} + \frac{1}{gA} \frac{\partial Q}{\partial t} + \frac{\lambda Q|Q|}{2gDA^2} = 0 \\ \frac{\partial h}{\partial t} + \frac{a^2}{gA} \frac{\partial Q}{\partial x} = 0 \end{cases} \quad (3.1)$$

These governing equations describe the control volume dx , respectively:

- the conservation of mass (continuity equation)
- the conservation of momentum

Here, h is the piezometric head, Q is the volumetric flow rate, A is the cross-sectional area, D is the pipe diameter, λ is the Darcy-Weisbach friction coefficient, g is gravity, and a is the wave speed.

As seen before, it is beneficial to adopt an electrical analogy. This approach allows us to interpret pressure (or piezometric head) as analogous to voltage, and discharge as analogous to current. This analogy leads to intuitive circuit-like representations of pipelines and hydraulic components, enabling the use of well-established analytical and numerical tools from circuit theory.

Following this analogy, we define the following parameters that represent hydraulic resistance, inertia, and capacitance, respectively:

$$R(Q_i) = \frac{\lambda |Q_i| dx}{2gDA^2}, \quad L = \frac{dx}{gA}, \quad C = \frac{gA dx}{a^2}$$

Here:

- $R(Q_i)$ models head loss due to friction and is nonlinear in flow
- L captures fluid inertia (analogous to inductance),
- C represents the ability of the pipe and fluid to store energy elastically (analogous to capacitance).

Discretization of the Continuity Equation

We begin by discretizing the continuity equation:

$$\frac{\partial h}{\partial t} + \frac{a^2}{gA} \frac{\partial Q}{\partial x} = 0 \quad (3.2)$$

Applying finite differences:

$$\left. \frac{\partial Q}{\partial x} \right|_i \approx \frac{Q_{i+1} - Q_i}{dx}, \quad \left. \frac{\partial h}{\partial t} \right|_i = \frac{dh_i}{dt} \quad (3.3)$$

Substituting and simplifying:

$$\frac{dh_i}{dt} = \frac{1}{C}(Q_i - Q_{i+1}) \quad (3.4)$$

Discretization of the momentum equation

For the momentum equation, we use centered finite differences in space:

$$\left. \frac{\partial h}{\partial x} \right|_i \approx \frac{h_{i+1} - h_{i-1}}{2dx}, \quad \left. \frac{\partial Q}{\partial t} \right|_i = \frac{dQ_i}{dt} \quad (3.5)$$

Substituting into the PDE:

$$\frac{h_{i+1} - h_{i-1}}{2dx} + \frac{1}{gA} \frac{dQ_i}{dt} + \frac{\lambda Q_i |Q_i|}{2gDA^2} = 0 \quad (3.6)$$

Multiplying through by dx :

$$\frac{h_{i+1} - h_{i-1}}{2} + \frac{dx}{gA} \frac{dQ_i}{dt} + \frac{\lambda Q_i |Q_i| dx}{2gDA^2} = 0 \quad (3.7)$$

Using the definitions of inductance L and resistance $R(Q_i)$, we obtain:

$$\frac{dQ_i}{dt} = -\frac{R(Q_i)}{L} Q_i - \frac{1}{L} \left(\frac{h_{i+1} - h_{i-1}}{2} \right) \quad (3.8)$$

With directional approximation:

$$\frac{h_{i+1} - h_{i-1}}{2} \approx \begin{cases} h_i - h_{i-1} & \text{for } Q_i \\ h_i - h_{i+1} & \text{for } Q_{i+1} \end{cases} \quad (3.9)$$

We derive the system:

$$\begin{aligned} \frac{dQ_i}{dt} &= -\frac{R(Q_i)}{L} Q_i - \frac{2}{L} h_i + \frac{2}{L} h_{i-1} \\ \frac{dQ_{i+1}}{dt} &= -\frac{R(Q_i)}{L} Q_{i+1} + \frac{2}{L} h_i - \frac{2}{L} h_{i+1} \end{aligned} \quad (3.10)$$

Final Discretized System

The final set of ODEs is:

$$\begin{aligned} \frac{dQ_i}{dt} &= -\frac{R(Q_i)}{L} Q_i - \frac{2}{L} h_i + \frac{2}{L} h_{i-1} \\ \frac{dQ_{i+1}}{dt} &= -\frac{R(Q_i)}{L} Q_{i+1} + \frac{2}{L} h_i - \frac{2}{L} h_{i+1} \\ \frac{dh_i}{dt} &= \frac{1}{C} (Q_i - Q_{i+1}) \end{aligned} \quad (3.11)$$

As we can see, this discretization corresponds to a single control volume i within the penstock. To describe the entire pipe, the penstock is divided into I

finite elements, each of equal length $dx = \frac{l}{I}$, where l is the total penstock length. Each element contributes three state variables:

- Q_i : discharge entering the control volume from the upstream side
- Q_{i+1} : discharge exiting the control volume toward the downstream side
- h_i : piezometric head at the center of the control volume

The resulting structure yields a total of $2I + 1$ state variables: $I + 1$ discharges and I heads. This setup is based on the Equivalent Electric Circuit (EEC) analogy, where each element is modeled as a third-order RLC circuit. The resistance $R(Q_i)$ represents frictional losses, the inductance L models the inertial effects of the fluid, and the capacitance C accounts for the compressibility of water and elasticity of the pipe walls.

This 1D representation is suitable for simulating wave propagation along the penstock with low computational cost. However, to ensure numerical stability, the time step dt used in the solver must satisfy the Courant–Friedrichs–Lewy (CFL) condition:

$$dt < \frac{dx}{a} \quad (3.12)$$

where a is the wave speed in the pipe. This condition guarantees that information does not propagate faster than physically allowed within the discretized domain.

The following Figure 3.1 and Figure 3.2 represent the RLC circuit for a penstock of i elements, and i -th element.

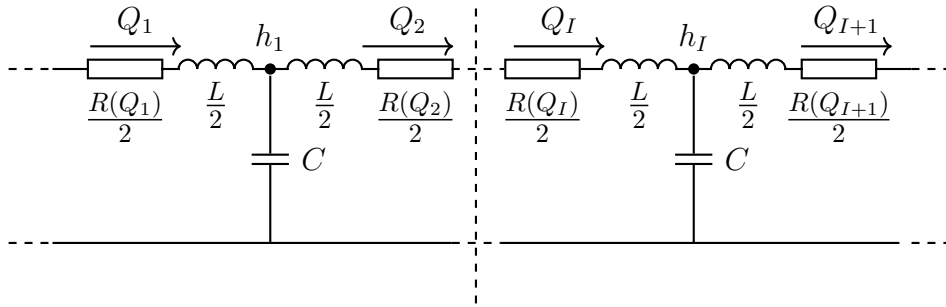


Figure 3.1: Penstock of i elements

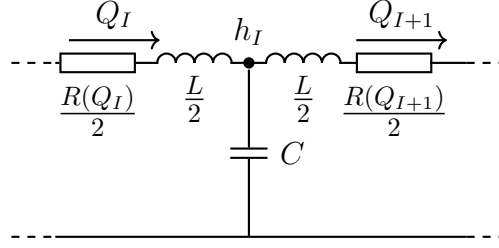


Figure 3.2: Single i-th segment

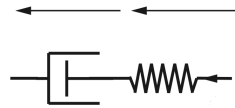
3.1.2 Viscoelastic Effects in the Penstock

Actually, the penstock pipe is not a perfectly rigid and purely elastic system. In abrupt transients, the structural response of the pipe wall becomes very critical, especially in dense fluid or high-pressure operating conditions. The pipe exhibits time-dependent deformation behavior, which is termed viscoelastic.

There are several rheological models that are commonly used to simulate interactions of this type, each joining springs and dashpots in a different configuration to simulate different time-dependent behaviors. [2]:

- The **Maxwell model**, with a spring and dashpot in series, suitable for modeling stress relaxation.
- The **Kelvin–Voigt model**, with a spring and dashpot in parallel, ideal for modeling creep and instantaneous damping.

Maxwell Model



Kelvin–Voigt Model

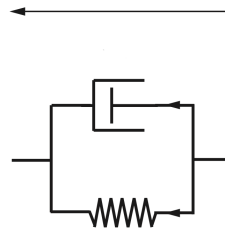


Table 3.1: Comparison of common rheological models: Maxwell and Kelvin–Voigt.

In this work, we adopt the Kelvin–Voigt model due to its simplicity and suitability for time-domain simulation of hydraulic transients. It introduces damping directly into the pressure–flow relationship, without requiring additional internal state variables.

To capture the complete viscoelastic behavior in our hydraulic system, we implement a model with **two Kelvin–Voigt branches in parallel**. This approach, following the methodology in [2], allows us to represent:

- the viscoelasticity of the pipe wall (structural deformation),
- the viscoelasticity of the fluid (compressibility and internal friction).

Each branch contributes independently to the overall pressure–flow response, and their combination gives a more accurate representation of energy storage and dissipation in the system.

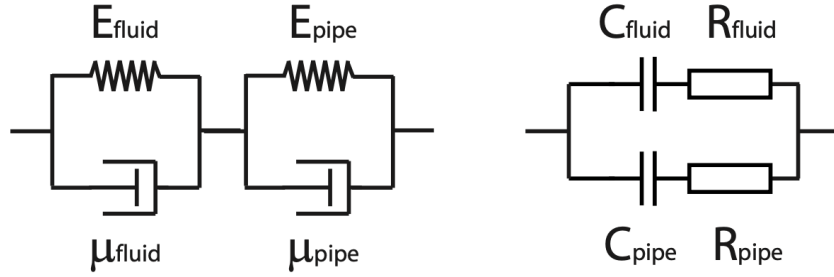


Figure 3.3: Schematic of the dual Kelvin–Voigt model used: two branches in parallel for pipe and fluid viscoelasticity.

3.1.2.1 From Elastic to Viscoelastic Pipe Models

The classical model of a pipe is based on elastic behavior and is derived from the momentum and continuity equations. In the 1D case, it can be represented by a RLC circuit analogy. The governing relation between piezometric head $h(t)$ and discharge $Q(t)$ is:

$$\frac{dh}{dt} = \frac{1}{C}(Q_i - Q_{i+1}) \quad \text{with} \quad C = \frac{gA\Delta x}{a^2} \quad (3.13)$$

This model assumes that pressure variations cause instantaneous elastic deformation in the pipe wall and compress the fluid volume. However, this neglects damping due to internal material resistance and time-dependent response.

To better capture fast transients and damping behavior, particularly in high-density fluids or polymer-based pipes, the pipe is extended using, as seen before, a Kelvin–Voigt model, which introduces time-dependent (viscous) deformation.

3.1.2.2 Kelvin–Voigt Model from Rheology to Hydraulics

The Kelvin–Voigt model describes viscoelastic materials by combining a spring (elastic component) and a dashpot (viscous component) in parallel. When applied to pipe walls, this formulation captures both immediate elastic deformation and time-dependent damping behavior. The constitutive law is:

$$\sigma(t) = E \cdot \epsilon(t) + \mu \cdot \frac{d\epsilon(t)}{dt} \quad (3.14)$$

where:

- $\sigma(t)$ is the applied stress,
- $\epsilon(t)$ is the strain (relative deformation),
- E is the Young’s modulus (elastic stiffness),
- μ is the viscoelastic damping coefficient.

To apply this model to a hydraulic system, we reinterpret these quantities:

- Strain $\epsilon(t)$ becomes the relative volume change of the fluid or the pipe wall:
 $\epsilon(t) = \frac{V(t)}{V_0}$
- Stress $\sigma(t)$ is associated with internal pressure, and by extension, piezometric head: $\sigma(t) = \rho g \cdot h(t)$
- The time derivative of strain is the rate of volume change, or flow: $\frac{d\epsilon(t)}{dt} = \frac{Q(t)}{V_0}$

Substituting these expressions into the Kelvin–Voigt model gives:

$$\rho g \cdot h(t) = E \cdot \frac{V(t)}{V_0} + \mu \cdot \frac{Q(t)}{V_0} \quad (3.15)$$

Solving for $h(t)$, we obtain:

$$h(t) = \frac{E}{\rho g V_0} \cdot V(t) + \frac{\mu}{\rho g V_0} \cdot Q(t) \quad (3.16)$$

This shows that the head depends both on how much volume has been stored in the system (elastic term), and on the instantaneous flow rate (viscous term). We now define:

$$\frac{1}{C} = \frac{E}{\rho g V_0}, \quad R = \frac{\mu}{\rho g V_0}$$

to obtain the compact hydraulic expression:

$$h(t) = \frac{1}{C} \cdot V(t) + R \cdot Q(t) \quad (3.17)$$

Since the stored volume is itself the time-integral of flow:

$$V(t) = \int_0^t Q(t) dt \quad (3.18)$$

we can rewrite the full model in terms of $Q(t)$ only:

$$h(t) = \frac{1}{C_{\text{pipe}}} \int_0^t Q(t) dt + R_{\text{pipe}} \cdot Q(t) \quad (3.19)$$

and in differential form:

$$\frac{dh}{dt} = \frac{1}{C} Q(t) + R \frac{dQ(t)}{dt} \quad (3.20)$$

This is the hydraulic form of the Kelvin–Voigt model. It captures both energy storage via the elastic term $\frac{1}{C} \int Q$, and energy dissipation via the viscous term RQ . The two parameters C and R encapsulate the physical and geometric properties of the pipe wall and fluid, and they form the basis for introducing viscoelasticity into the momentum equation of the pipeline model. where $Q_p(t) = \frac{dV}{dt}$ is the volumetric deformation rate (stored flow). The coefficients are defined as:

$$C_{\text{pipe}} = \frac{AD\rho g dx}{E_{\text{pipe}} e}, \quad R_{\text{pipe}} = \frac{\mu_{\text{pipe}} e}{AD\rho g dx}$$

The same reasoning applies to the fluid’s compressibility and viscosity, leading to a second Kelvin–Voigt branch[3]:

$$C_{\text{fluid}} = \frac{A\rho g dx}{E_{\text{fluid}}}, \quad R_{\text{fluid}} = \frac{\mu_{\text{fluid}}}{A\rho g dx}$$

Equivalent Viscoelastic Model: C_{ve} and R_{ve} The total viscoelastic effect is modeled by combining the pipe and fluid Kelvin–Voigt branches in parallel. This results in an equivalent model characterized by:

$$C_{ve} = C_{\text{pipe}} + C_{\text{fluid}} = A\rho g dx \left(\frac{D}{E_{\text{pipe}}e} + \frac{1}{E_{\text{fluid}}} \right)$$

$$\frac{1}{R_{ve}} = \frac{1}{R_{\text{pipe}}} + \frac{1}{R_{\text{fluid}}} \Rightarrow R_{ve} = \frac{\mu_{\text{equiv}}}{A\rho g dx}$$

$$\mu_{\text{equiv}} = \left(\frac{1}{\mu_{\text{pipe}} \cdot \frac{e}{D}} + \frac{1}{\mu_{\text{fluid}}} \right)^{-1}$$

The capacitance C_{ve} matches the classical expression used in the elastic pipe model:

$$C = \frac{gA dx}{a^2}$$

but now a series resistance R_{ve} appears, which captures the viscoelastic damping behavior absent in purely elastic models.

3.1.2.3 Numerical Form of the Viscoelastic Model

The viscoelastic formulation introduces a first-order time-dependent effect into the model. While the classical elastic relation between head and flow at node i is:

$$\frac{dh_i}{dt} = \frac{1}{C}(Q_i - Q_{i+1}) \quad (3.21)$$

the Kelvin–Voigt-enhanced model accounts for both storage and damping, we can do this with Equations (3.19) and (??):

$$h_i(t) = \frac{1}{C} \int (Q_i - Q_{i+1}) dt + R_{ve} \cdot (Q_i - Q_{i+1}) \quad (3.22)$$

or equivalently, in differential form:

$$\frac{dh_i}{dt} = \frac{1}{C}(Q_i - Q_{i+1}) - \frac{R_{ve}}{C} \cdot \frac{d(Q_i - Q_{i+1})}{dt} \quad (3.23)$$

This additional term introduces dynamic damping that smooths rapid transients and improves numerical stability.

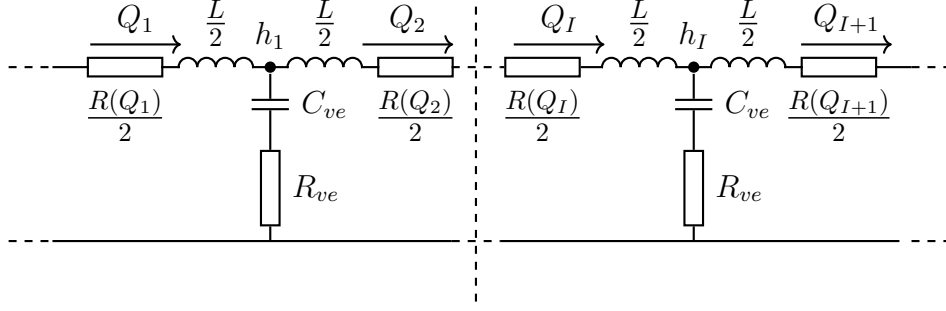


Figure 3.4: Penstock of i elements

Interpretation of R_{ve} and C_{ve}

- C_{ve} : represents the elastic energy storage capacity due to both the pipe wall and the fluid. It defines the propagation speed of pressure waves and matches the classical capacitance expression.
- R_{ve} : quantifies the viscoelastic damping introduced by pipe and fluid behavior. It acts as a smoothing resistance that damps high-frequency components and stabilizes the numerical solution.

3.1.2.4 Impact on Wave Propagation and Damping

The viscoelasticity introduces a modification to the propagation of the pressure wave down the penstock. The viscoelastic model introduces the following over purely elastic models:

- Attenuation of wave velocity through the introduced effective capacitance
- Energy losses over time through the viscoelastic resistive elements
- Smoothed-out pressure fronts and high damping frequencies

These effects become highly significant in simulations with dense fluids or high-velocity transients, where pressure waves would otherwise reflect rigidly at boundaries or produce unstable numerical artifacts. The modified system is a more accurate model of true hydraulic behavior, especially in components like the T-branch where geometry, fluid properties, and wall flexibility all contribute to dynamic damping.

3.2 Valve

3.2.1 Modeling as Static or Dynamic Boundary Condition

Valves introduce pressure losses in hydraulic systems due to flow constriction and turbulence. These losses depend on the valve geometry and its degree of opening, which is described by the obturator position s . The valve can be modeled as a nonlinear resistive element, either at a boundary or as part of an internal network element. The modeling starts from the classical Bernoulli principle.

Bernoulli Principle Between two points in steady, incompressible, inviscid flow along a streamline, the total mechanical energy per unit weight is conserved:

$$\frac{p_1}{\rho g} + \frac{v_1^2}{2g} + z_1 = \frac{p_2}{\rho g} + \frac{v_2^2}{2g} + z_2 + H_{\text{loss}} \quad (3.24)$$

Here, H_{loss} accounts for energy dissipation due to turbulence, geometry changes, and other effects such as friction or localized contractions. For a valve, the main cause of energy loss is the abrupt contraction and turbulence downstream of the throttling element.

Head Loss Due to a Valve For a local loss such as a valve, the pressure drop is related to the flow velocity by:

$$H_v = \frac{K_v(s)}{2g} \cdot v^2 \quad (3.25)$$

where:

- H_v : head loss across the valve [m],
- v : flow velocity through the valve opening [m/s],
- $K_v(s)$: dimensionless loss coefficient, depending on the valve opening s .

To express the head loss in terms of the discharge Q , we introduce the cross-sectional reference area A_{ref} , assumed constant for the system:

$$v = \frac{Q}{A_{\text{ref}}} \Rightarrow H_v = \frac{K_v(s)}{2g} \cdot \left(\frac{Q}{A_{\text{ref}}} \right)^2 = \frac{K_v(s)}{2g A_{\text{ref}}^2} \cdot Q^2 \quad (3.26)$$

This yields the final expression used to model head losses across a valve:

$$H_v = \frac{K_v(s)}{2gA_{\text{ref}}^2} \cdot Q^2 \quad (3.27)$$

Nonlinear Resistance Interpretation The valve can also be represented as a variable hydraulic resistance, by analogy with Ohm's law, relating head drop and flow:

$$H_v = R_v(s) \cdot Q \quad \text{with} \quad R_v(s) = \frac{K_v(s)}{2gA_{\text{ref}}^2} \cdot |Q| \quad (3.28)$$

This formulation highlights the nonlinear character of the valve: the resistance depends both on the magnitude of flow and on the valve position. This model is particularly convenient for integration in time-domain simulations, as it treats the valve as a memoryless, static nonlinear element unless dynamic actuator models are added.

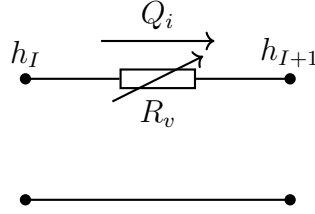


Figure 3.5: Regulated resistor coupling between h_I and h_{I+1}

3.3 Surge Tank

3.3.1 Capacitive and Resistive Behavior in the T-Branch

The surge tank is a free-surface reservoir connected to the main pressurized pipeline. It plays a key role in transient hydraulic behavior by absorbing or supplying fluid depending on system conditions. Its dynamics are governed by conservation of volume and localized head losses at the connection point.

Capacitive Behavior from Volume Balance The volume of water stored in the surge tank at any time t can be expressed as:

$$V_{\text{st}}(t) = \int A(z) dz \quad (3.29)$$

where $A(z)$ is the cross-sectional area as a function of vertical coordinate z . Differentiating with respect to time yields the flow rate entering or leaving the tank:

$$\frac{dV_{\text{st}}}{dt} = A(z) \cdot \frac{dz}{dt} \quad (3.30)$$

Recognizing that the variation in volume corresponds to the exchanged discharge Q_c , and introducing the piezometric head $h_c(t)$ as the vertical water level, we obtain:

$$A(z) \cdot \frac{dh_c}{dt} = Q_c(t) \quad (3.31)$$

This is the general capacitive behavior of the surge tank, where the area may vary with height. For tanks with constant cross-section A_{st} , this simplifies to:

$$\frac{dh_c}{dt} = \frac{1}{A_{\text{st}}} \cdot Q_c(t) \quad (3.32)$$

We then define the hydraulic capacitance as:

$$C_{\text{st}} = A_{\text{st}} \quad (3.33)$$

Resistive Behavior from Localized Losses At the junction between the surge tank and the pipeline, flow undergoes localized losses due to abrupt entry/exit conditions. According to Bernoulli's principle, these losses are expressed as:

$$\Delta h_r(t) = \frac{K_{\text{st}}}{2gA_{\text{ref}}^2} \cdot Q_c(t)^2 \quad (3.34)$$

This leads to a nonlinear resistance of the form:

$$R_{\text{st}}(Q) = \frac{K_{\text{st}}}{2gA_{\text{ref}}^2} \cdot |Q| \quad (3.35)$$

$$\Delta h_r(t) = R_{\text{st}}(Q) \cdot Q_c(t) \quad (3.36)$$

Total Head and Flow Balance The piezometric head at the surge tank connection is the sum of the internal tank level and the head drop across the entrance:

$$h_{st}(t) = h_c(t) + \Delta h_r(t) \quad (3.37)$$

Flow continuity at the T-branch gives the local Kirchhoff relation:

$$Q_I = Q_{I+1} + Q_c \quad (3.38)$$

Equivalent RC Representation The surge tank is thus modeled as an RC element:

- A **capacitor** C_{st} representing free-surface storage,
- A **nonlinear resistor** $R_{st}(Q)$ capturing entrance/exit losses.

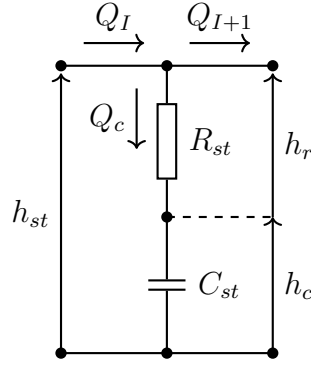


Figure 3.6: Capacitor–resistor representation of the surge tank in the T-branch.

3.4 Turbines

Hydraulic turbines are key elements in a hydropower plant, responsible for converting the energy stored in the fluid into mechanical rotational power. The basic output power of a turbine can be estimated from the Bernoulli principle, assuming ideal conversion of potential and kinetic energy into mechanical work. The hydraulic power available to the turbine is expressed as:

$$P_{hyd} = \rho g h Q \quad (3.39)$$

where:

- ρ is the fluid density [kg/m³],
- g is the gravitational acceleration [m/s²],
- h is the net head across the turbine [m],
- Q is the volumetric flow rate [m³/s].

To account for real-world performance losses (mechanical friction, turbulence, blade efficiency), we introduce a performance coefficient η , also known as the turbine efficiency. Therefore, the actual mechanical power output of the turbine becomes:

$$P_{\text{out}} = \eta \rho g h Q \quad (3.40)$$

In our 1D hydraulic model, we use this simplified expression to model the turbine as an energy extraction element. Control dynamics, guide vane positioning, and generator coupling are outside the scope of this model but are discussed in more detailed sources such as [4].

3.4.1 Turbine Types

Different turbine types are optimized for different hydraulic conditions such as head and flow rate. Below we summarize three of the most common turbine designs:

3.4.1.1 Francis Turbine

The Francis turbine is a reaction turbine with radial and axial flow. It is widely used in medium head (40 to 400 meters) and medium flow applications. Its design allows for good efficiency and operational flexibility.

3.4.1.2 Pelton Turbine

The Pelton turbine is an impulse turbine ideal for high head (above 300 meters) and low flow conditions. Water jets hit spoon-shaped buckets attached to the runner, converting kinetic energy into rotation without submerging the runner.

3.4.1.3 Kaplan Turbine

The Kaplan turbine is an axial-flow reaction turbine designed for low head (below 40 meters) and high flow applications. It features adjustable blades, making it very efficient in variable load conditions such as in run-of-river plants.

Turbine Type	Head Range	Flow Range	Application Example
Francis	40–400 m	Medium	Most medium-scale hydropower plants
Pelton	>300 m	Low	Mountainous or high-altitude plants
Kaplan	<40 m	High	Run-of-river or flat terrain HPPs

Table 3.2: Comparison of common hydraulic turbines

This categorization helps guide turbine selection during plant design depending on the site’s elevation profile and water availability.

Chapter 4

State-Space Representation of the HPP System

4.1 From Discretized PDEs to State Equations

As introduced in Chapter 2, one-dimensional (1D) models provide a practical trade-off between accuracy and computational speed for simulating hydraulic transients in Hydropower Plants (HPPs). These models are especially valuable for real-time applications such as monitoring, diagnosis, and control design. They capture the essential dynamics of the water column using the analogy of electrical circuits, discretizing the penstock into a series of segments characterized by inertia, elasticity, and friction. This approach leads naturally to a system of first-order Ordinary Differential Equations (ODEs), which can be expressed in state-space form.

To derive this formulation, the penstock is divided into I segments. Each segment is modeled using a parameter approach with five main physical quantities used as input:

- Q_i : the volumetric flow rate entering segment i
- Q_{i+1} : the flow exiting segment i
- h_i : the pressure head at the center of segment i
- h_{i-1} : the pressure head at the upstream node of segment i
- h_{i+1} : the pressure head at the downstream node of segment i

Using the conservation of momentum and mass, the dynamics of each segment can be expressed as:

$$\frac{dQ_i}{dt} = -\frac{R(Q_i)}{L}Q_i + \frac{2}{L}(h_{i-1} - h_i) \quad (4.1)$$

$$\frac{dQ_{i+1}}{dt} = -\frac{R(Q_{i+1})}{L}Q_{i+1} + \frac{2}{L}(h_i - h_{i+1}) \quad (4.2)$$

$$\frac{dh_i}{dt} = \frac{1}{C}(Q_i - Q_{i+1}) \quad (4.3)$$

These equations are linearized around an operating point, resulting in a linear time-invariant system suitable for state-space modeling:

$$\dot{x} = Ax + Bu \quad (4.4)$$

where x is the state vector composed of flow and head variables, u is the input vector (e.g., reservoir and turbine heads), A is the system matrix capturing internal dynamics, and B defines how inputs affect the states.

4.2 Building the System Matrix

The dynamic behavior of the penstock can be described by a set of first-order differential equations [5] derived from the conservation of mass and momentum. When discretized into I segments using the equivalent circuit analogy, the model yields a state-space representation of the form:

$$\dot{x} = A(Q_i) \cdot x + B \cdot u$$

where:

- $x \in \mathbb{R}^{2I+1}$ is the state vector containing flow and pressure head variables:

$$x = \begin{bmatrix} Q_1 & Q_2 & \cdots & Q_{I+1} & h_1 & h_2 & \cdots & h_I \end{bmatrix}^T$$

- $u \in \mathbb{R}^2$ is the input vector:

$$u = \begin{bmatrix} h_0 \\ h_{I+1} \end{bmatrix}$$

representing the upstream reservoir head and downstream turbine/discharge head.

- $A(Q_i) \in \mathbb{R}^{(2I+1) \times (2I+1)}$ is the system matrix, which depends on the flow rates Q_i due to the nonlinear friction term $R(Q_i)$.
- $B \in \mathbb{R}^{(2I+1) \times 2}$ maps the boundary conditions into the system.

The generalized structure of the system matrix A and input matrix B is:

$$A = \begin{bmatrix} -R(Q_1)/L & 0 & 0 & 0 & -2/L & 0 & 0 & 0 & 0_{1,2I+1} \\ 0 & -R(Q_2)/L & 0 & 0 & 1/L & -1/L & 0 & 0 & 0 \\ 0 & 0 & \ddots & 0 & 0 & \ddots & \ddots & 0 & 0 \\ 0 & 0 & 0 & -R(Q_{I+1})/L & 0 & 0 & 1/L & -1/L & 0 \\ 0_{I+1,1} & 0 & 0 & 0 & 0 & 0 & 0 & 2/L & 0 \\ 1/C & -1/C & 0 & 0 & 0 & 0 & 0 & 0 & 0 \\ 0 & \ddots & \ddots & 0 & 0 & 0 & 0 & 0 & 0 \\ 0_{2I+1,1} & 0 & 1/C & -1/C & 0 & 0 & 0 & 0 & 0 \end{bmatrix}$$

$$[B] = \begin{bmatrix} 2/L & 0 \\ 0 & 0 \\ 0 & 0 \\ 0_{I,1} & -2/L \\ 0 & 0 \\ 0_{I+1,1} & 0 \end{bmatrix}$$

This structure reflects the local coupling between adjacent flow and head variables:

- Each flow Q_i is affected by the friction loss $R(Q_i)$ and the difference in adjacent heads.
- Each pressure head h_i accumulates mass from the difference between inflow and outflow.

In the next section, we will describe how to extend this formulation to include additional hydraulic elements such as valves, surge tanks, and viscoelastic damping.

4.3 Boundary Conditions and System Initialization

In any dynamic simulation of a hydraulic system, a natural question arises:

Do we need to explicitly initialize the internal state variables such as flows Q_i and pressure heads h_i ?

The answer lies in how we define the input vector and apply boundary conditions.

In our state-space formulation, the internal dynamics of the penstock are determined entirely by the initial state $x(0)$ and the evolution of the input vector $u(t)$, which captures the upstream and downstream heads:

$$u(t) = \begin{bmatrix} h_0(t) \\ h_{I+1}(t) \end{bmatrix}$$

These two boundary values are "drives" on the system. Upstream head h_0 is generally constant and considered as a large reservoir, and h_{I+1} is the tailwater or the pressure head from the turbine. Since these heads are imposed externally, they are not part of the state vector and do not require differential equations.

As initialization:

- If the simulation is initiated at steady state, $x(0)$ should be chosen so that it fulfills $\dot{x} = 0$, that is, solving the steady-state version of the system.
- If a transient is being modeled (e.g., the transient following a valve closure or surge tank), then any steady-state initial condition $x(0)$ can be chosen because the model will evolve based on the defined input $u(t)$.

Therefore, the boundary conditions not only dictate the evolution of the system but also physically determine the interpretation of the simulation indirectly: flow into and out of the penstock is regulated by applied head difference at the boundary. It allows internal flows and pressures to be specified dynamically without imposing any additional constraints.

4.4 Coupling Hydraulic Elements

The modular structure of the state-space model makes it naturally extendable to more complex configurations. In particular, we distinguish two ways of coupling new hydraulic components into the system matrix A :

- **Horizontal coupling:** modification of existing rows in A , without increasing the number of states. This corresponds to elements such as valves, which introduce additional pressure drops or flow restrictions between existing nodes.

- **Vertical coupling:** addition of new states (i.e., extra rows and columns in A), representing the dynamics of the added component. This is the case for surge tanks or viscoelastic effects that require modeling the evolution of new physical quantities (e.g., tank head or intermediate flows).

Example of Horizontal Coupling: Valve between nodes h_1 and h_2

We consider a simplified penstock divided into two segments, resulting in three flow states Q_1, Q_2, Q_3 and two pressure head states h_1, h_2 . A valve is inserted between nodes h_1 and h_2 , meaning it affects the flow Q_2 in the middle of the penstock.

The pressure loss introduced by the valve is originally nonlinear, but it can be linearized around an operating point Q_0 as:

$$\Delta h_{\text{valve}} \approx \frac{K_v |Q_0|}{2gA_{\text{ref}}^2} Q_2$$

This additional pressure drop modifies the momentum equation for Q_2 . Originally:

$$\frac{dQ_2}{dt} = -\frac{R(Q_2)}{L} Q_2 + \frac{2}{L} (h_1 - h_2)$$

becomes:

$$\frac{dQ_2}{dt} = -\left(\frac{R(Q_2)}{L} + \frac{K_v |Q_0|}{2gA_{\text{ref}}^2 L} \right) Q_2 + \frac{2}{L} (h_1 - h_2)$$

The modified diagonal entry in matrix A corresponding to the flow state Q_2 becomes:

$$A_{Q_2, Q_2} = -\left(\frac{R(Q_2)}{L} + \frac{R_v}{L} \right)$$

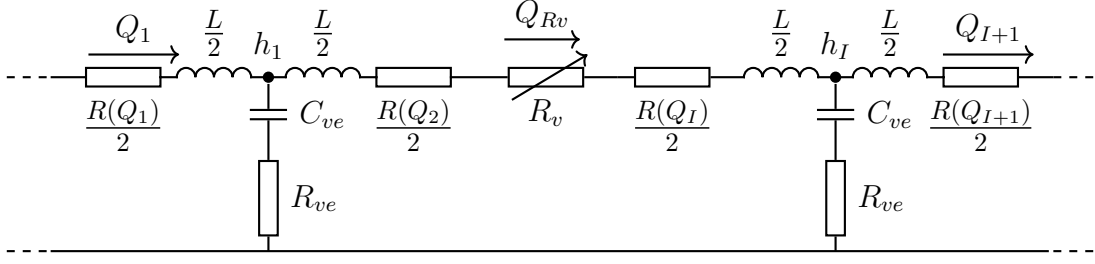
where R_v is the linearized resistance introduced by the valve, defined as:

$$R_v = \frac{K_v |Q_0|}{2gA_{\text{ref}}^2}$$

Here, Q_0 is the nominal operating point around which the flow Q_2 is linearized. This expression allows the valve's nonlinear head loss to be approximated by a constant resistance in the state-space model.

The structure of the model is preserved, and no new states are added.

The electrical scheme results in:


 Figure 4.1: Valve between nodes h_1 and h_I

And the A matrix:

$$A = \begin{bmatrix} -R(Q_1)/L & 0 & 0 & -2/L & 0 & 0 \\ 0 & -(R(Q_2)/L + \frac{R_v}{L}) & 0 & 1/L & -1/L & 0 \\ 0 & 0 & -R(Q_3)/L & 0 & 2/L & 0 \\ 0 & 0 & 0 & 0 & 2/L & 0 \\ 1/C & -1/C & 0 & 0 & 0 & 0 \\ 0 & 1/C & -1/C & 0 & 0 & 0 \end{bmatrix}$$

Example of Vertical Coupling: Surge Tank between Nodes h_1 and h_3

We consider a simplified penstock divided into two segments, with flow states Q_1, Q_2, Q_{2-st}, Q_3 and pressure head states h_1, h_{st}, h_3 . A surge tank is connected at the T-junction between the two pipe segments, where the flow Q_2 from the upstream side splits into Q_{2-st} toward the turbine and Q_{st} into the surge tank.

The surge tank is modeled as a resistive-capacitive (RC) pair. It introduces one new state variable:

- h_{st} : pressure head at the surge tank connection

The flow into the tank is governed by the pressure difference between the tank surface (assumed at known height h_c) and the T-junction head h_{st} , through a nonlinear resistance:

$$R_{st}(Q_{st}) = \frac{K_d(Q_{st})}{2gA_{\text{ref}}^2} \cdot |Q_{st}|$$

This leads to the pressure drop:

$$\Delta h = R_{st}(Q_{st}) \cdot Q_{st}$$

and the relation at the T-junction becomes (as seen in 3.4.1):

$$h_{st} = h_c + R_{st}(Q_{st}) \cdot Q_{st}$$

The net flow into the tank is given by the flow imbalance at the T-junction:

$$Q_{st} = Q_{2-st} - Q_2$$

Since the head in the tank is assumed constant at h_c , the surge tank does not introduce a dynamic equation for h_c . Instead, it modifies the pressure at the node h_{st} algebraically, depending on the flow imbalance and the resistive loss:

$$h_{st} = h_c + R_{st}(Q_{2-st} - Q_2) \cdot (Q_{2-st} - Q_2)$$

To incorporate this into the state-space model:

- One new head state h_{st} is added to the state vector:

$$x = \begin{bmatrix} Q_1 & Q_2 & Q_{2-st} & Q_3 & h_1 & h_{st} & h_3 \end{bmatrix}^T$$

- The continuity equation at h_{st} is modified to account for the flow into the surge tank:

$$\frac{dh_{st}}{dt} = \frac{1}{A_{st}} Q_{st} = \frac{1}{A_{st}} (Q_{2-st} - Q_2)$$

- This results in a new row in the matrix A corresponding to h_{st} , with:

$$A_{h_{st}, Q_{2-st}} = +\frac{1}{A_{st}}, \quad A_{h_{st}, Q_2} = -\frac{1}{A_{st}}$$

No modifications are made to the momentum equations for Q_2 or Q_{2-st} , but the head value at h_{st} is now influenced by both the surge tank and the adjacent flows.

This vertical coupling increases the system order by one and reflects the energy storage behavior of the tank.

This is the electrical scheme:

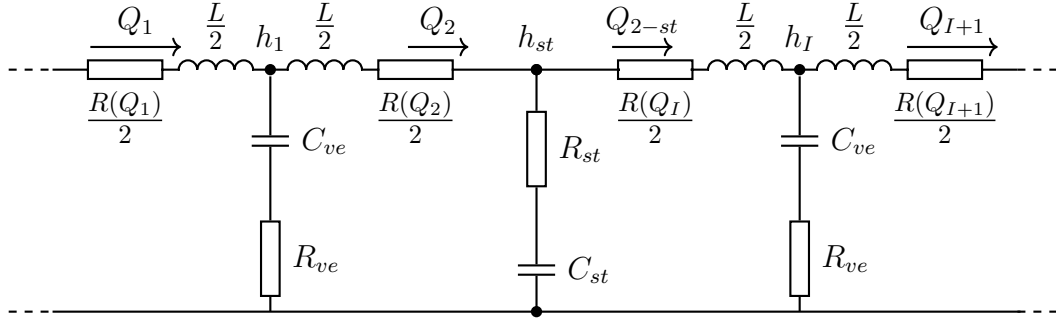


Figure 4.2: Surge tank in between nodes h_1 and h_I

And the A matrix:

$$A_{surge} = \begin{bmatrix} -R(Q_1)/L & 0 & 0 & 0 & -2/L & 0 & 0 & 0 & 0 & 0 & 0 \\ 0 & -R(Q_2)/L & 0 & 0 & 1/L & -1/L & 0 & 0 & 0 & 0 & 0 \\ 0 & 0 & \ddots & 0 & 0 & \ddots & \ddots & 0 & 0 & 0 & 0 \\ 0 & 0 & 0 & -R(Q_{I+1})/L & 0 & 0 & 1/L & -1/L & 0 & 0 & 0 \\ 0 & 0 & 0 & 0 & 0 & 0 & 0 & 2/L & 0 & 0 & 0 \\ 1/C & -1/C & 0 & 0 & 0 & 0 & 0 & 0 & -1/C & 0 & 0 \\ 0 & \ddots & \ddots & 0 & 0 & 0 & 0 & 0 & 0 & 0 & 0 \\ 0 & 0 & 1/C & -1/C & 0 & 0 & 0 & 0 & 0 & 0 & 0 \\ 0 & 0 & 0 & 0 & 0 & 1/L_{st} & 0 & 0 & -R_{st}/L_{st} & -1/L_{st} & 0 \\ 0 & 0 & 0 & 0 & 0 & 0 & 0 & 0 & 1/A_{st} & 0 & 0 \end{bmatrix}$$

Chapter 5

Fluid Density Considerations

The density of the working fluid is a fundamental property that directly influences the performance of hydropower systems. While water is typically assumed to have constant density in most conventional analyses, real-world scenarios may involve fluids of different densities due to dissolved substances or experimental setups. Variations in density affect the energy content per unit volume of the fluid, and consequently, the power output of a HydroPower Plant (HPP). Since the hydraulic power is proportional to the product of density, gravitational acceleration, volumetric flow rate, and head, even modest changes in density can translate into measurable changes in turbine output. This chapter introduces the importance of accounting for fluid density in system modeling and sets the stage for a deeper investigation into how key parameters must be adjusted accordingly.

5.1 Effect of Variable Density on System Behavior

In dynamic fluid systems such as those in HPPs, changing the fluid density alters the system's inertia, the pressure response to transient events, and the way energy is transmitted and dissipated. These changes affect both steady-state and transient behavior. In particular, wave propagation through the hydraulic circuit, the effective pressure head, and internal friction losses all respond to modifications in fluid density. Recognizing and modeling these effects accurately is essential for reliable simulation and control of the plant.

5.2 Parameters that Need Adjustment

Three primary parameters require correction when the density of the working fluid changes:

- **Wave speed (a):** The celerity of pressure waves in a pipe depends on both the fluid's bulk modulus and its density. When density increases, wave speed typically decreases, which modifies the time scales of pressure transients and water hammer effects.
- **Head (h):** The pressure head, traditionally defined as the potential energy per unit weight of fluid, varies linearly with density when measured in terms of energy per unit volume. Consequently, a change in density alters the energy content at a given geometric height, and thus the mechanical power that can be extracted.
- **Reynolds number and Darcy–Weisbach friction factor (Re and λ):** These parameters govern the viscous losses in the system. Since Reynolds number is inversely proportional to viscosity and directly proportional to density and velocity, a denser fluid at the same velocity leads to a higher Reynolds number, potentially shifting the flow regime and altering the friction factor λ .

5.3 Candidate Fluids and Feasibility

Not all dense fluids are viable for hydropower applications. While increasing density enhances power output, it also introduces technical and economic constraints. The following table summarizes several candidate fluids, along with their densities and a brief discussion of their suitability.

As the table shows, although many dense fluids exist, very few are practical for hydropower. Most are either too expensive or hazardous. The only realistic candidates are purpose-designed mineral solutions, like those being developed for closed-loop pumped hydro systems. From this point forward, we will focus our analysis on feasible fluids such as R-19, a experimental and functional fluid used in some HPPs [6][10], and saturated brines (e.g. Cs-formate and $ZnBr_2$),

5.3. Candidate Fluids and Feasibility

Fluid	Density (kg/m ³)	Feasibility and Applications
Water (H ₂ O)	1000	Standard in all HPPs. Safe, cheap, abundant.
Proprietary Mineral Solution (e.g. R-19)	2500	Used in closed-loop pumped hydro. Non-toxic, high performance [6].
Saturated Brines (e.g. Cs-formate, ZnBr ₂)	2200–2300	Used in oil/gas wells. Corrosive, expensive, sealed systems only [7].
Diiodomethane (CH ₂ I ₂)	3300	Lab use only. Toxic and unstable [8].
Gallium or Galinstan	5900–6400	Liquid metals. Very expensive, niche cooling uses [9].
Mercury (Hg)	13600	Extremely toxic. Historic lab use only.

Table 5.1: Comparison of Fluid Densities for Hydropower Use

which offer high density with acceptable levels of safety and applicability in sealed environments.

Chapter 6

Wave Speed in Hydraulic Transients

6.1 Introduction

Wave speed, or wave celerity, is defined as the speed at which a pressure disturbance propagates through a fluid-filled conduit. In the context of transient hydraulic phenomena such as water hammer, wave speed determines how quickly changes in pressure and flow rate travel along the pipeline. Physically, it represents the velocity of elastic waves in the fluid–pipe system.

Wave speed is more than a physical property; it is a critical parameter in mathematical models of hydraulic systems. It appears in the governing equations of motion for unsteady flow and plays a major role in determining pressure surges, simulation timing, and numerical stability.

6.2 Role of Wave Speed in Hydropower Modelling

In pumped-storage or conventional hydropower plants, wave speed governs the dynamic interaction between the reservoir, penstock, and turbine during transient events. A higher wave speed results in faster propagation of pressure changes, which can intensify surge effects and increase the risk of overpressure or underpressure conditions. This results in lower wave speeds that indicate a more compliant

system that attenuates the pressure waves more gradually.

In numerical simulations, wave speed determines the Courant number as seen in Eq. (3.12):

$$C_n = \frac{a \Delta t}{\Delta x} \quad (6.1)$$

where a is wave speed, Δt is the time step, and Δx is the spatial discretization. For numerical accuracy and stability, it is generally required that $C_n = 1$. However, since different sections of the hydraulic system can have different wave speeds, achieving a common time step across the entire network becomes difficult. This is especially relevant when modeling a complete hydropower plant where pipes vary in material, diameter, and boundary conditions.

6.3 Basic Wave Speed Formula

In a rigid pipe with compressible fluid, the wave speed is given by the acoustic velocity:

$$a_0 = \sqrt{\frac{K}{\rho}} \quad (6.2)$$

where:

- K is the bulk modulus of the fluid [Pa],
- ρ is the fluid density [kg/m³].

This equation represents the theoretical maximum wave speed in a system without pipe wall deformation. For water at 20°C, $K \approx 2.07 \times 10^9$ Pa and $\rho \approx 1000$ kg/m³, resulting in $a_0 \approx 1440$ m/s.

In real pipes, the pipe wall deforms under pressure, absorbing some of the wave energy. The extended wave speed formula, considering pipe elasticity, is:

$$a = \sqrt{\frac{K}{\rho \left(1 + \frac{KD}{Ee}\right)}} \quad (6.3)$$

where:

- E is Young's modulus of the pipe material [Pa],
- D is the internal pipe diameter [m],
- e is the pipe wall thickness [m].

6.4 Corrected Formula and Pipe Support Coefficient

Nevertheless, it is needed in HPPs to take into account the support of the pipe since we are working on big models. The refined formula accounts this through the correction factor ψ :

$$a = \sqrt{\frac{K}{\rho \left(1 + \frac{KD\psi}{Ee}\right)}} \quad (6.4)$$

The coefficient ψ varies based on how the pipe is restrained axially. This includes Poisson's ratio ν , the e/D ratio, and the specific support configuration. In [11] it provides the following cases:

Case 1: Anchored at upstream end only

$$\psi = \frac{1}{1 + e/D} \left[\frac{5}{4} - \nu + 2\frac{e}{D}(1 + \nu) \left(1 + \frac{e}{D}\right) \right] \quad (6.5)$$

Case 2: Fully anchored pipe (no axial movement)

$$\psi = \frac{1}{1 + e/D} \left[1 - \nu^2 + 2\frac{e}{D}(1 + \nu) \left(1 + \frac{e}{D}\right) \right] \quad (6.6)$$

Case 3: Pipe with expansion joints

$$\psi = \frac{1}{1 + e/D} \left[1 + 2\frac{e}{D}(1 + \nu) \left(1 + \frac{e}{D}\right) \right] \quad (6.7)$$

Case	Support Condition	Typical ψ Approximation
1	Anchored at one end	$\approx 1.25 - \nu$
2	Fully anchored	$\approx 1 - \nu^2$
3	With expansion joints	≈ 1.0

Table 6.1: Summary of ψ values for typical support conditions

6.5 Assumptions and Limitations

The wave speed expressions used above rely on the following assumptions:

- **Thin-walled pipe:** Valid for $D/e > 25$ –40.
- **No cavitation:** The pipe remains fully filled with fluid, and pressure does not fall below the vapor pressure.
- **Low air content:** The fluid is homogeneous and the bulk modulus remains constant during transients.
- **Negligible pipe inertia:** No transverse vibration or axial motion of the pipe is considered.
- **Uniform pressure across cross-section:** The flow is treated as one-dimensional.

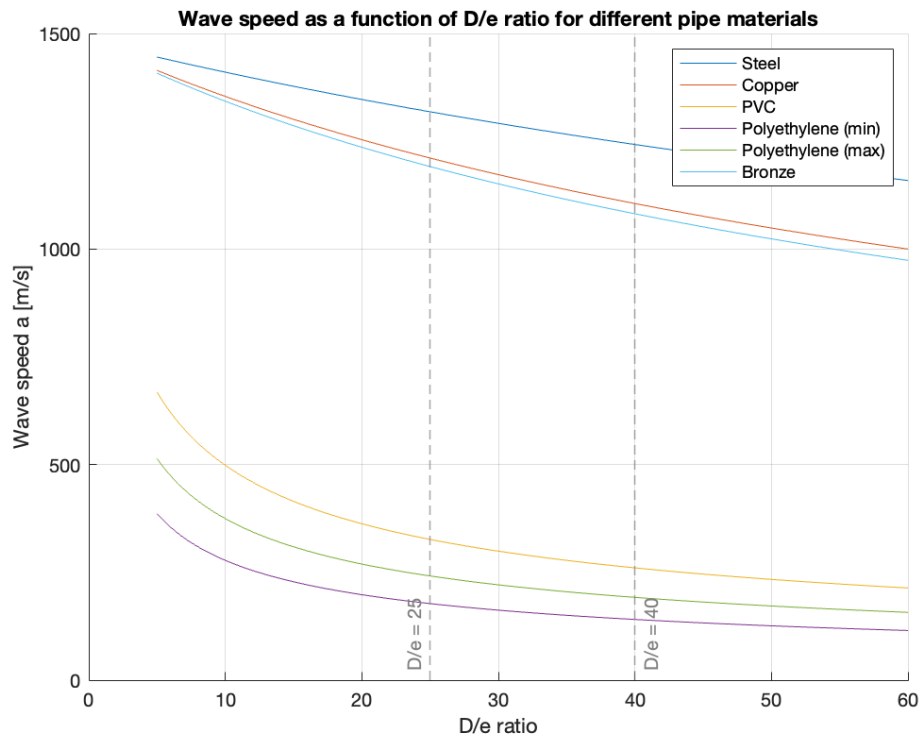


Figure 6.1: Wave speed as a function of D/e ratio for different pipe materials.

In Figure 6.1 we can see how a higher D/e ratio results in a lower wave speed and stabilizes the rate at which it decreases ($n^{\circ 1}$ assumption of a thin-walled pipe). So for stability purposes and benefits on the modeling, a higher D/e ratio can help adjusting the parameters

6.6 Wave Speed in Different Pipe Materials

Pipe material strongly influences wave speed through its modulus of elasticity E and Poisson's ratio ν . The table below presents typical values and corresponding wave speed ranges. Nevertheless, this study aims on re powering existing HPPs and no reconstruction is expected.

Material	E [GPa]	ν	Typical a [m/s]
Steel	207	0.30	1200–1300
Copper	110	0.36	1000–1200
PVC	2.8	0.45	250–500
Polyethylene	0.8–1.5	0.46	100–300
Bronze	100	0.34	950–1150

Table 6.2: Typical wave speeds for different pipe materials

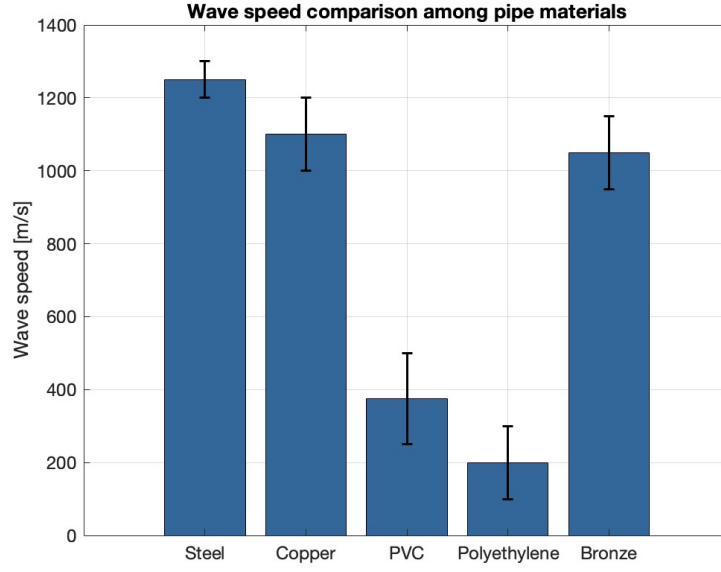


Figure 6.2: Wave speed comparison among materials.

6.7 Comparison of Wave Speeds and Courant Numbers for Different Fluids

Now, to understand the impact of fluid properties on transient modeling, we compare the wave speeds resulting from different fluid densities, using Eq.(6.4) with typical material parameters for a standard steel pipe.

Let us consider the three fluids:

- **Water (baseline):** $\rho = 1000 \text{ kg/m}^3$
- **R-19 mineral solution:** $\rho = 2500 \text{ kg/m}^3$
- **Saturated brines (e.g. ZnBr_2):** $\rho = 2200 \text{ kg/m}^3$

6.7. Comparison of Wave Speeds and Courant Numbers for Different Fluids

Holding all other terms constant, the increase in fluid density reduces the wave speed a , since $a \propto 1/\sqrt{\rho}$. This has two major effects:

1. **Numerical implications:** Lower wave speed permits larger time steps Δt for a fixed Courant number $C_n = 1$. This is beneficial for simulation efficiency.
2. **Physical interpretation:** A denser, slower-propagating wave front results in a more damped system response, with slower transient behavior.

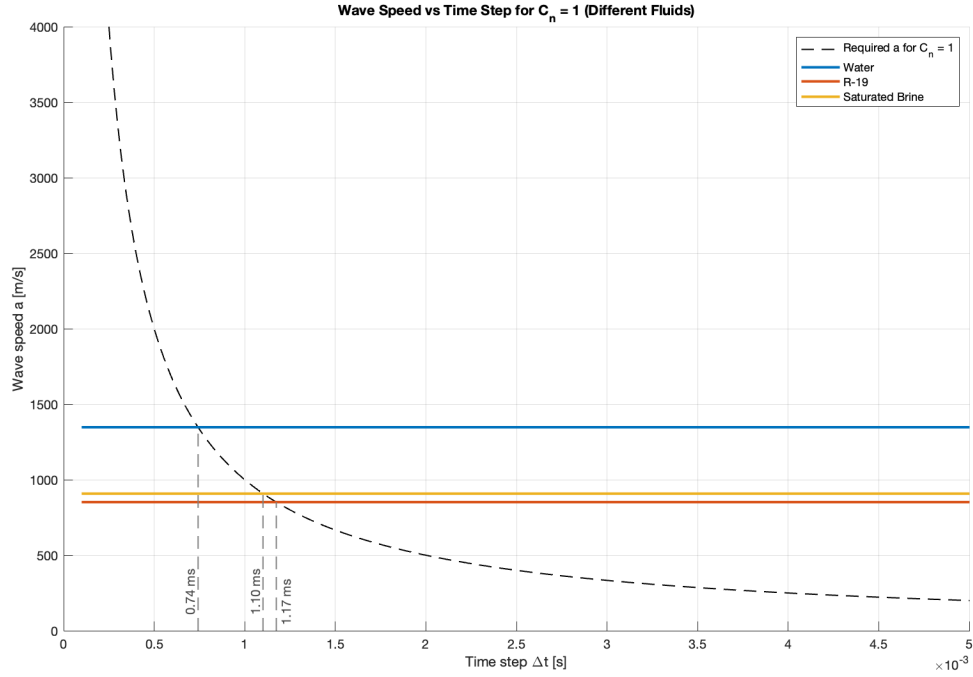


Figure 6.3: Wave speed and Courant number comparison for Water, R-19, and Saturated Brine in a steel pipe.

Looking at Figure 6.3 it is possible to see the relation between wave speed and time step for a Courant number $C_n = 1$, in a comparison among three fluids: Water, R-19, and Saturated Brine. The dashed line is the wave speed required to maintain $C_n = 1$ as a function of the time step. Horizontal lines indicate the

wave speed for each fluid in a steel pipe. Notably, lower wave velocities of denser fluids such as R-19 and Saturated Brine support larger stable time steps. For instance, R-19 with a wave speed of approximately 889, m/s can have a time step of approximately 1.17, ms, in contrast to water with a wave speed of 1350, m/s and a time step of 0.74, ms. This amounts to an increase in allowable time step by 58.1% and significantly decreases the number of iterations contained within a numerical simulation and therefore the total computational cost. Hence, use of higher-density fluids can yield practical advantages when real-time or high-speed simulation performance is critical.

6.8 Conclusion

Wave speed is a core parameter in the modeling of hydraulic transients. It explains the interaction between fluid compressibility, pipe elasticity, and structural restraint where accurate estimation is vital for reliable simulation, safe design, and transient analysis. As seen, a lower wave speed gives the opportunity of a higher time step and a faster simulation. Nevertheless, while simplified adjustments may be useful in practice, they must be scrutinized for physical realism, especially in high-performance systems such as hydropower plants.

Chapter 7

Hydraulic Head and Fluid Density

7.1 Definition and Physical Meaning of Hydraulic Head

Hydraulic head is a measure of the potential energy available in a fluid due to its pressure and elevation, and velocity. In hydropower systems, it quantifies the energy per unit weight of fluid that can be converted into mechanical and then electrical energy. For incompressible fluids under static or slow-moving conditions, the hydraulic head is typically dominated by pressure and elevation terms, and is defined by:

$$h = \frac{p}{\rho g} \quad (7.1)$$

where:

- h is the hydraulic head [m]
- p is the pressure [Pa]
- ρ is the fluid density [kg/m³)]
- g is the gravitational acceleration (typically 9.81 m/s²).

7.2 Dependence of Head on Fluid Density

From the equation above, it is clear that for the same pressure p , the hydraulic head h is inversely proportional to fluid density ρ . A denser fluid generates the same pressure with a lower elevation difference. On the other hand, for a fixed head h and flow rate Q , the power output increases linearly with fluid density:

$$P = \rho g Q h \quad (7.2)$$

This indicates that a denser fluid results in a higher mechanical power output from the same flow and head.

7.3 Recalculating Head for Non-Water Fluids

To analyze the impact of using a denser fluid, consider a fluid with density ρ_f replacing water (ρ_w). The hydraulic head required to produce the same pressure becomes:

$$h_f = \frac{p}{\rho_f g} = \frac{\rho_w}{\rho_f} h_w \quad (7.3)$$

This means that for a fluid twice as dense as water, the same pressure can be achieved with half the elevation.

7.3.1 Example: Recomputing $h = 320$ m for Higher-Density Fluid

Let us suppose a high-density fluid, like R-19, with $\rho_f = 2500$ kg/m³ is used in place of water ($\rho_w = 1000$ kg/m³). To maintain the same pressure at the turbine inlet, the new head h_f that yields the same pressure as $h_w = 320$ m of water is:

$$h_f = \frac{\rho_w}{\rho_f} \cdot h_w = \frac{1000}{2500} \cdot 320 = 128 \text{ m} \quad (7.4)$$

This means that the same pressure (and therefore the same energy per unit volume) can be achieved with only 128 m of head using the denser fluid. However, what happens to the power output?

Hydraulic power is given, as seen before, by:

$$P = \rho g Q h \quad (7.5)$$

Substituting the head expression:

$$P = \rho g Q \cdot \frac{p}{\rho g} = Q p \quad (7.6)$$

This shows that if pressure p and flow rate Q are kept constant (h is reduced due to needing lower altitude for the same pressure), the power output remains unchanged regardless of fluid density. In this case, even though head decreases as density increases, power does not change because the energy per unit volume of fluid (i.e. pressure) stays the same.

But the key comes if the geometric head h is kept constant (e.g. using a 320 m elevation drop with a denser fluid), then the power output increases proportionally with density:

$$P \propto \rho \quad (\text{if } h, Q \text{ fixed}) \quad (7.7)$$

This distinction is critical in hydropower design. In closed-loop systems where the head is fixed by terrain or infrastructure, increasing fluid density is an effective way to boost output. But if the goal is to maintain the same pressure level (and reduce infrastructure height), then the net power output remains the same.

7.4 Implications for System Design and Control

Using denser fluids in hydropower systems yields several benefits and challenges:

- **Increased Power Output:** Since $P = \rho g Q h$, increasing ρ directly increases the output power. A fluid 2.5 times denser than water yields 2.5 times the power for the same head and flow.
- **Reduced Infrastructure Requirements:** With higher density, the required head for a given pressure or power output is reduced. This enables hydropower installations on low-elevation terrains.
- **Higher Pressure Loads:** For the same head, denser fluids exert more pressure. Pipes, turbines, and valves must be engineered to withstand greater forces, increasing material and maintenance requirements.

7.5 Graphical Comparison of Head for Different Fluids

To visualize the effect of fluid density on the required hydraulic head, we will include a comparative figure showing how the head varies for different working fluids at constant pressure. This will help demonstrate how infrastructure requirements can be optimized through fluid selection.

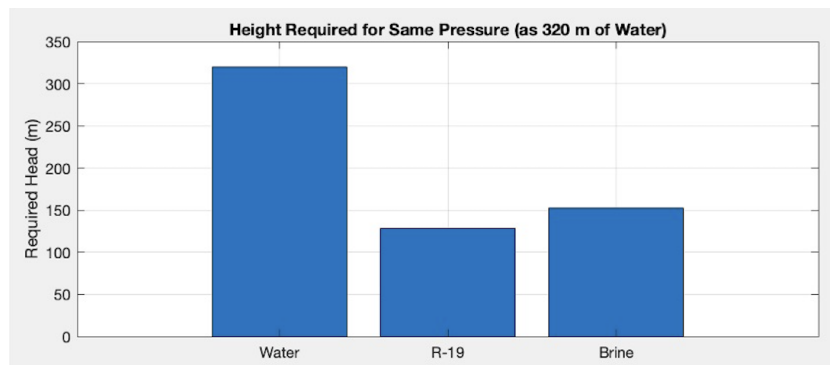


Figure 7.1: Comparison of required head h for different fluids at constant pressure.

This graphical analysis reinforces the practical benefit of using high-density fluids in closed-loop pumped hydro applications, where reducing head directly reduces civil engineering costs while maintaining the same energy output or results in a higher power output maintaining the same head drop.

Chapter 8

Friction Factor and Reynolds Number Analysis

When analyzing penstock performance, it is crucial to understand how the flow regime (laminar vs. turbulent flow) is characterized by the Reynolds number, and how this in turn affects the friction factor (often denoted λ) used in head loss calculations. This chapter provides a theoretical analysis of these concepts, covering flow regime classification by Reynolds number, the need for local calculations along a discretized penstock model, the iterative determination of friction factor via the Darcy–Weisbach equation, and the influence of fluid properties and pipe roughness on frictional losses.

8.1 Determining the Flow Regime

The Reynolds number (Re) is a dimensionless quantity that determines the flow regime. It is defined as:

$$Re = \frac{\rho V D}{\mu} \quad (8.1)$$

where ρ is the fluid density, V is the average flow velocity, D is the pipe diameter, and μ is the dynamic viscosity.

The flow regime is classified as follows:

Flow Regime	Reynolds Number Range
Laminar	$\text{Re} < 2300$
Transitional	$\text{Re} \approx 2300\text{--}4000$
Turbulent	$\text{Re} > 4000$

Table 8.1: Flow regime classification by Reynolds number

In laminar flow, viscous forces dominate and the velocity profile is parabolic. In turbulent flow, inertial forces dominate and the profile is flatter due to eddies and mixing. The transitional regime is unpredictable and must be handled carefully in modeling.

To capture the behavior of the flow accurately, especially when diameter or velocity varies, the Reynolds number should be computed locally:

$$\text{Re}_i = \frac{\rho V_i D_i}{\mu}, \quad \forall i \in \{1, \dots, n\}, \quad (8.2)$$

where subscript i refers to the local section of the penstock. This reinforces the need for spatial discretization in penstock models.

8.2 Friction Factor Models

The Darcy–Weisbach equation describes the head loss due to friction:

$$h_{f,i} = \lambda_i \frac{L_i}{D_i} \frac{V_i^2}{2g}, \quad \text{or in terms of } Q_i : \quad (8.3)$$

$$h_{f,i} = \lambda_i \frac{L_i}{D_i} \frac{1}{2g} \left(\frac{4Q_i}{\pi D_i^2} \right)^2, \quad (8.4)$$

$$h_{f,i} = \lambda_i \frac{L_i}{D_i} \frac{8Q_i^2}{\pi^2 D_i^4 g}. \quad (8.5)$$

where $h_{f,i}$ is the friction head loss for section i , λ_i is the Darcy friction factor, L_i is the section length, and g is the gravitational acceleration.

In laminar flow, the friction factor is given analytically as:

$$\lambda_i = \frac{64}{\text{Re}_i}. \quad (8.6)$$

For turbulent flow, λ_i depends on both Re_i and the relative roughness ε_i/D_i . The Colebrook–White equation is used:

$$\frac{1}{\sqrt{\lambda_i}} = -2 \log_{10} \left(\frac{\varepsilon_i/D_i}{3.7} + \frac{2.51}{\text{Re}_i \sqrt{\lambda_i}} \right). \quad (8.7)$$

This equation is implicit in λ_i and must be solved iteratively. A typical approximation such as the Swamee–Jain formula can also be used:

$$\lambda_i \approx \left[-1.325 \ln \left(\frac{\varepsilon_i/D_i}{3.7} + \frac{5.74}{\text{Re}_i^{0.9}} \right) \right]^{-2}. \quad (8.8)$$

Iterative Computation per Discretized Element

To model the penstock accurately, we consider a discretization into n segments. For each segment i , we apply the following iterative procedure:

1. **Initial guess:** Start with an initial guess for the friction factor, typically:

$$\lambda_i^{(0)} = 0.02. \quad (8.9)$$

2. **Velocity computation:** Assuming a known flow rate Q , compute the velocity in segment i using:

$$V_i^{(k)} = \frac{Q^{(k)}}{A_i} = \frac{4Q^{(k)}}{\pi D_i^2}, \quad (8.10)$$

where A_i is the cross-sectional area and k is the iteration index.

3. **Reynolds number:**

$$\text{Re}_i^{(k)} = \frac{\rho V_i^{(k)} D_i}{\mu}. \quad (8.11)$$

4. **Update friction factor:** Compute a new $\lambda_i^{(k+1)}$ using Colebrook–White or an explicit correlation (e.g. Swamee–Jain) based on $\text{Re}_i^{(k)}$ and ε_i/D_i .

5. **Convergence check:** Repeat steps 2–4 until:

$$|\lambda_i^{(k+1)} - \lambda_i^{(k)}| < \epsilon, \quad (8.12)$$

for a given tolerance ϵ , typically 10^{-6} .

6. **Update flow rate (if necessary):** If pressure drop or head is fixed and flow rate is unknown, update $Q^{(k+1)}$ based on total head loss and repeat for all segments.

This local iterative process must be applied for all $i = 1, \dots, n$ to account for geometry and material variations along the penstock.

8.3 Sensitivity to Friction Assumptions

Sensitivity analysis is essential when the system operates near the laminar–turbulent transition. The friction factor can vary significantly depending on the assumed regime. For example, if $\text{Re}_i = 1500$, then:

$$\lambda_i^{\text{laminar}} = \frac{64}{1500} \approx 0.042, \quad (8.13)$$

whereas a turbulent estimate might be:

$$\lambda_i^{\text{turbulent}} \approx 0.02. \quad (8.14)$$

This leads to large discrepancies in predicted head loss. Moreover, in transitional flow (typically Re between 2300 and 4000), the friction factor is highly sensitive and non-deterministic, needing either empirical correction or conservative design assumptions.

Additionally, the Reynolds number is directly proportional to fluid density and inversely proportional to viscosity:

$$\text{Re}_i = \frac{\rho V_i D_i}{\mu} \propto \frac{\rho}{\mu}, \quad (8.15)$$

so an increase in density raises Re_i , while an increase in viscosity reduces it. Therefore, a plant that is already designed for turbulent flow at a given fluid composition will continue to exhibit turbulence when simulated with a higher-density, lower-viscosity fluid. However, a change in viscosity or a combination

of both parameters can shift the flow toward the transitional regime, increasing sensitivity in the determination of λ .

8.3.1 Graphical Analysis of Density and Viscosity Effects on λ and Reynolds Number

To complement the theoretical framework and iterative friction modeling, we now present a graphical study that compares the behavior of the three different fluids under study: water, R-19, and Brine. These visualizations explore how fluid density ρ and viscosity μ influence the Reynolds number and the friction factor λ , and ultimately affect head losses along the penstock.

The Reynolds number is given by:

$$Re_i = \frac{\rho V_i D_i}{\mu} \propto \frac{\rho}{\mu}, \quad (8.16)$$

This equation highlights the two key variables in determining whether the flow is turbulent, transitional, or laminar. The following figures provide insight into the sensitivity of the system to these variables.

First of all, Figure 8.1, explains how the study should be done, since the model will only work if the entire penstock is under the same regime, turbulent or laminar. And if there is a change, the Re_i should be re calculated.

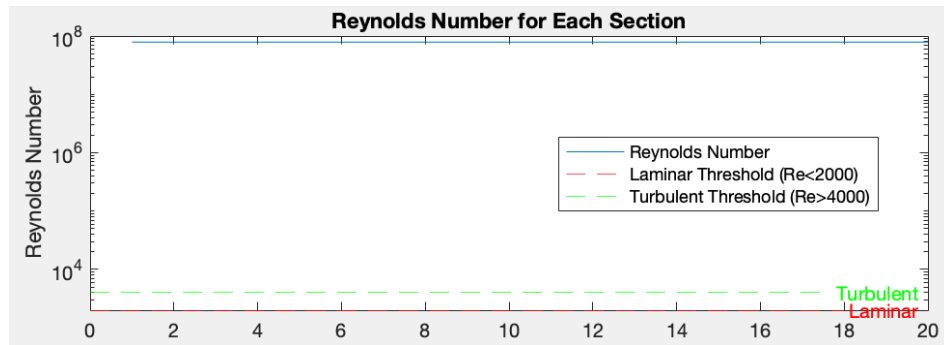
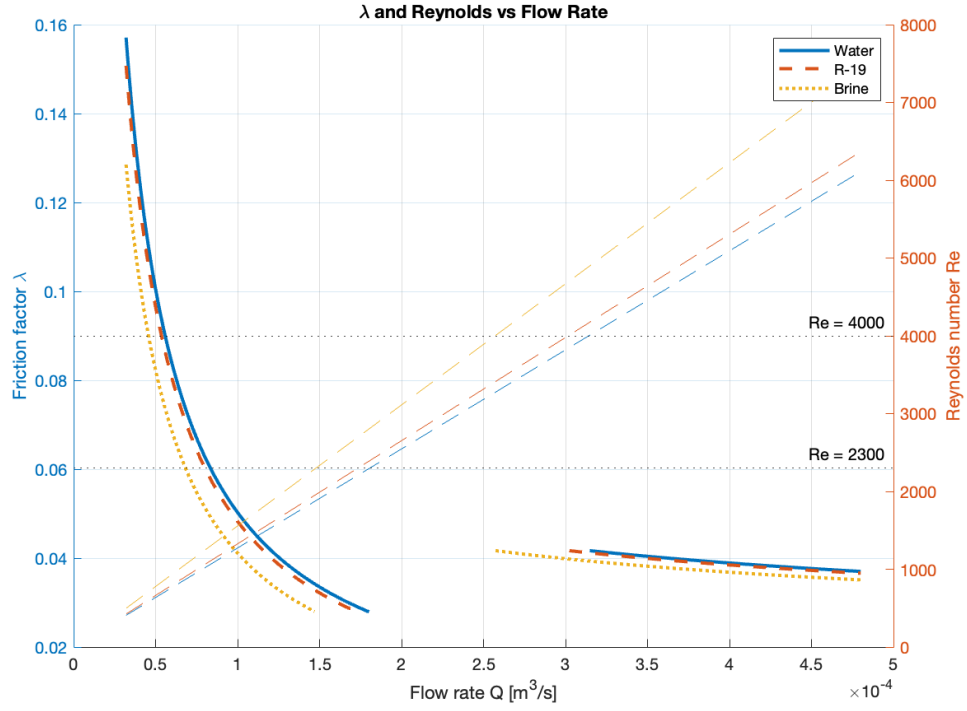
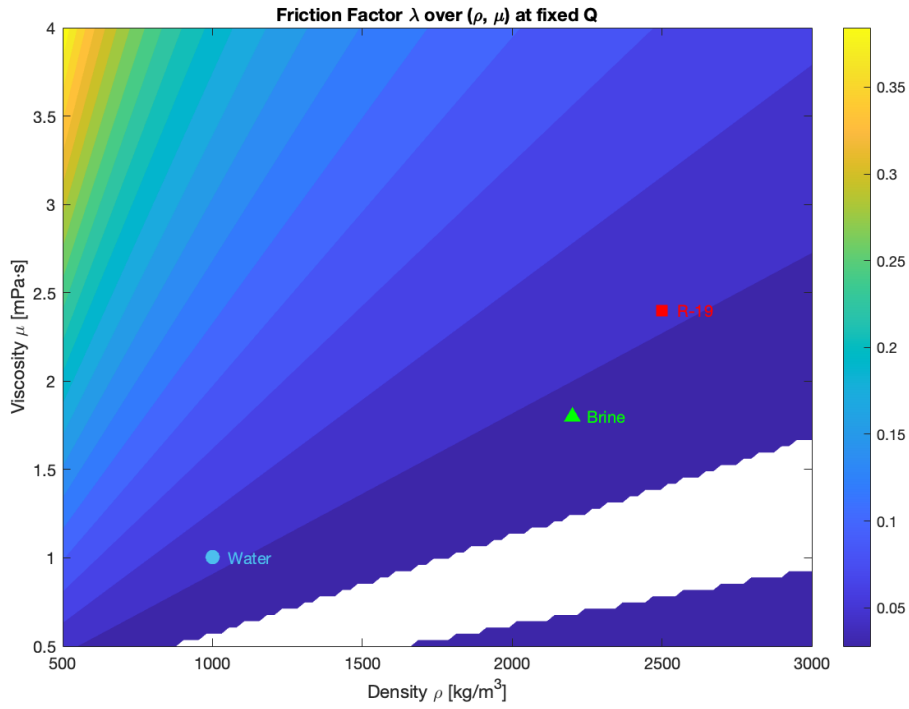


Figure 8.1: Values of Re_i per section and regime thresholds drawn.

As seen in Figure 8.1, this is a typical case where we have a high Reynolds number, this is due to using numbers from a real HPP where the values of Q and penstock parameters are huge.



(a) Friction factor λ and Reynolds number as a function of flow rate Q for Water, R-19, and Brine.



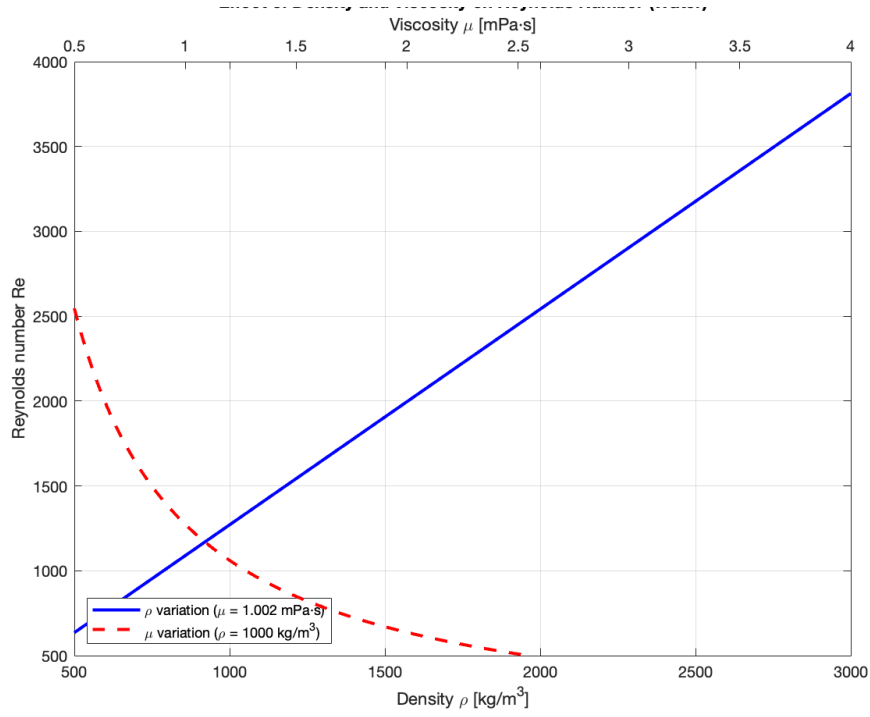
(b) Friction factor λ as a function of density ρ and viscosity μ at a fixed flow rate in turbulent regime. Markers indicate locations of Water, Brine, and R-19.

Figure 8.2: Figures (a) and (b): Influence of flow rate and fluid properties on λ and Reynolds number.

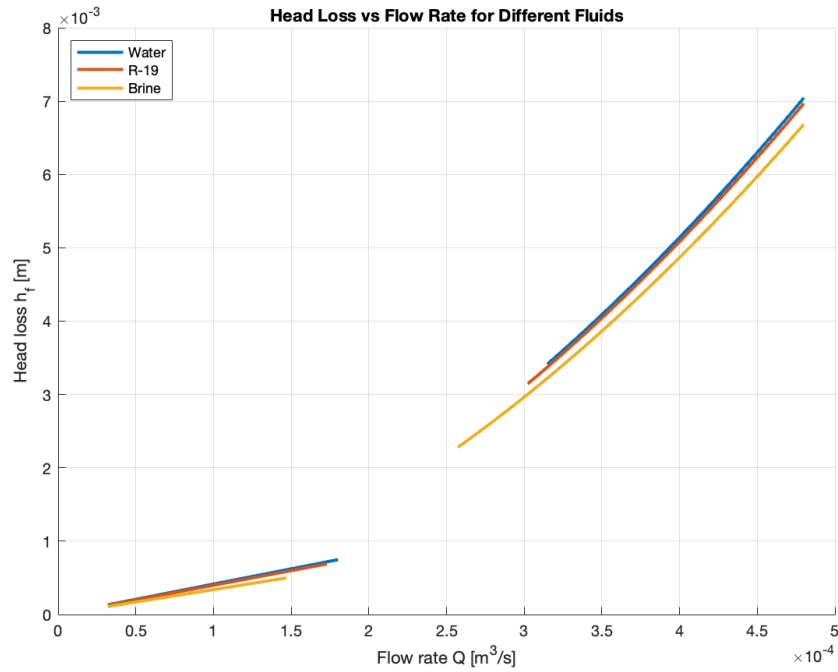
The following figures, reinforce the theoretical ideas seen before and how should we analyze each parameter regarding the Reynolds number and friction factor. In Figure 8.2a, the brighted colored curves show how the friction factor λ decreases as the flow rate Q increases. All fluids follow the expected turbulent trend, with λ decreasing more rapidly at low Q . We can also say the other feasible fluids are similiar to water regarding lambda, thus head losses. The dashed lines in the background represent the Reynolds number being the Brine the highest which combines high density with high viscosity.

Figure 8.2b offers a visual map of the friction factor λ over the density-viscosity plane for a fixed flow rate, in this case, turbulent flow. Each color band corresponds to a level of friction factor. This plot allows us to scatter and compare the fluids in terms of their effective hydraulic behavior. Fluids that fall within the same color region as Water are expected to experience similar frictional losses. For example, R-19 lies near Water, indicating similar λ values, while Brine is located in a lighter color band, suggesting lower friction. However, despite a potentially similar λ , fluids with higher density (such as R-19 or Brine) will produce a higher pressure head for the same geometric configuration. This makes the plot useful for identifying fluids that match water's performance or that may offer higher hydraulic head with comparable friction.

8.3. Sensitivity to Friction Assumptions



(a) Reynolds number vs. density and viscosity. Blue: ρ variation at constant μ , Red: μ variation at constant ρ .



(b) Head loss h_f versus flow rate Q for the three fluids.

Figure 8.3: Figures (a) and (b): Isolated effects of fluid properties and resulting head loss behavior.

Figure 8.3a isolates the individual influence of density and viscosity on the Reynolds number. The blue line illustrates a linear increase in Re as density ρ increases while keeping viscosity constant, confirming the proportionality predicted analytically. In contrast, the red dashed curve shows a steep nonlinear decline in Re as viscosity μ increases at constant density. This highlights the dominant role of viscosity in determining the flow regime: even small increases in μ can significantly reduce Re , potentially pushing the system into the transitional or laminar zone. Therefore, when selecting or comparing fluids for hydropower applications, special attention must be paid to viscosity, especially in regimes where Re is borderline.

Figure 8.3b translates the flow behavior into practical head loss values h_f as a function of flow rate Q . Interestingly, both Water and R-19 result in nearly identical head losses across the range of Q , despite R-19 having higher Reynolds numbers. This suggests that the net effect of R-19's high density and slightly higher λ balances out. Brine, on the other hand, shows consistently lower head losses due to its combination of high density and relatively low friction factor. These results indicate that Brine may offer hydraulic efficiency advantages under certain conditions, even if it does not reach the highest Re .

Together, these figures demonstrate how both fluid parameters, density and viscosity, significantly affect flow regime classification, frictional losses, and hydropower system performance. This graphical study strengthens the motivation for local analysis, in fluid-specific modeling in HPP simulations, especially when using non-standard working fluids.

Chapter 9

Simulation Results and Comparative Analysis

This chapter reports steady state results for a reference HPP using two working fluids: water and the high density fluid R-19 (as seen before where its density is higher and its characteristics are associated with water). The penstock and boundary conditions are identical in both cases so the geometric head is fixed by civil works. The objectives are to quantify the effect of fluid density on turbine power, the distribution of head along the penstock, and frictional losses, and to assess the energy benefit of using a denser fluid.

Table 9.1: Main characteristics of the reference plant.

Parameter	Value
Gross head H	320 m
Penstock length L	1100 m
Penstock diameter D	5 m
Pipe roughness ϵ	45×10^{-6} m
Design discharge Q	50 m ³ /s
Turbine efficiency η	90%
Flow assumption	Steady, fully developed
Segments for loss analysis	10

Table 9.2: Physical properties of the working fluids.

Fluid	Density ρ (kg/m ³)	Dynamic viscosity μ (Pa·s)
Water	1000	1.0×10^{-3}
R-19	2500	2.4×10^{-3}

9.1 Baseline Power Output with Water vs. R-19

The most direct effect of using a denser fluid is an increase in the mechanical power output at the turbine for the same flow and head conditions. Figure 9.1 compares the calculated turbine power for water and for R-19, assuming the gross head is fixed at 320 m and the flow is 50 m³/s in both cases. The turbine power P is obtained from the classic relation $P = \rho g Q H \eta$, where $\eta = 0.9$ is the turbine efficiency (assumed equal for both fluids). As expected, the heavier fluid delivers a dramatically higher power:

- **Water:** $P_{\text{water}} \approx 139$ MW (baseline)
- **R-19 fluid:** $P_{\text{R-19}} \approx 348$ MW

This corresponds to roughly a **150% increase** in output when using R-19 instead of water, for the same operating conditions. The gain is almost exactly proportional to the density ratio ($2500/1000 = 2.5$), reflecting the fact that the available potential energy per unit volume of fluid is higher.

9.2 Pressure (Head) Distribution Along the Penstock

We next examine the pressure profile (expressed as piezometric head h) along the penstock for both fluids. Figure 9.2 plots the steady-state head distribution from the reservoir (upstream end) to the turbine inlet (downstream end) for water and for R-19 at the full flow $Q = 50$ m³/s. The upstream reservoir head is approximately 320 m, and the downstream end (turbine wicket gate) is set as reference height 0 m with the remaining head representing pressure at the turbine inlet.

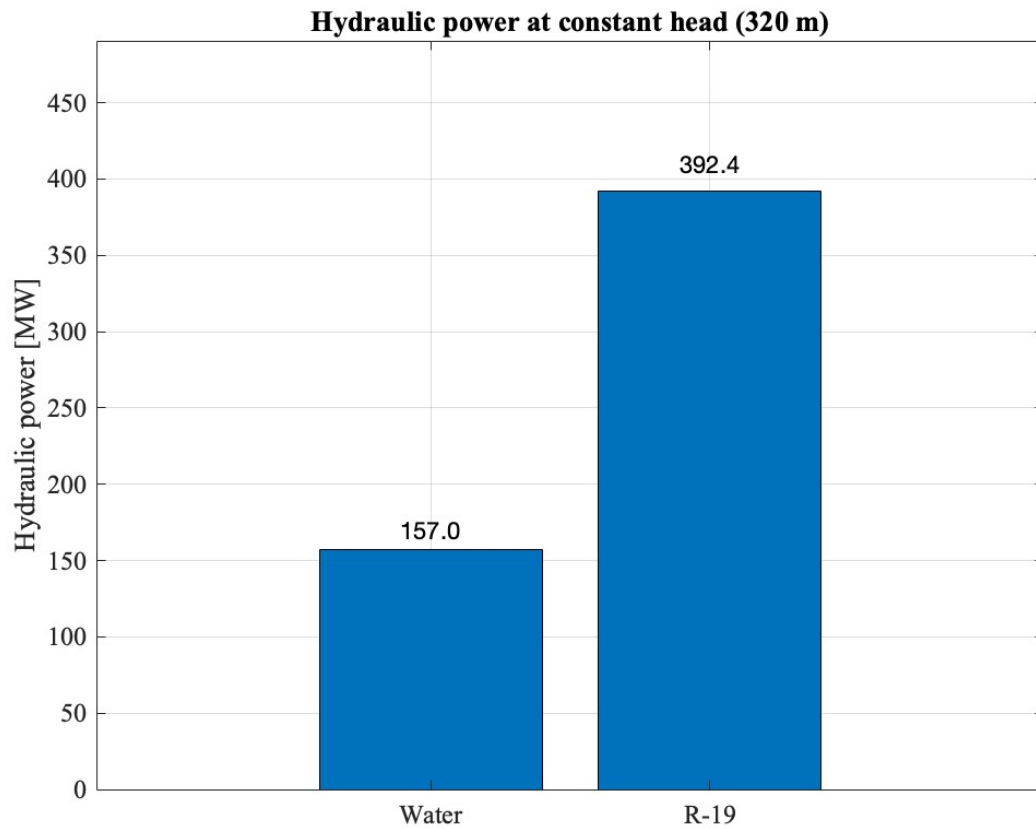


Figure 9.1: Turbine mechanical power output at a fixed head of 320 m for Water vs. R-19. The higher-density fluid delivers substantially greater power from the same head and flow rate, reflecting the proportional increase of $\rho g H$ available energy.

As shown in Figure 9.2, the head drops nearly linearly along the penstock for both fluids, indicating a uniform frictional gradient. Importantly, the R-19 curve is almost indistinguishable from the water curve, so both fluids lose on the order of only 0.6–0.7 m of head over the 1100 m pipe. This confirms that the introduction of a denser fluid does not significantly alter the distribution of head in the system under steady flow.

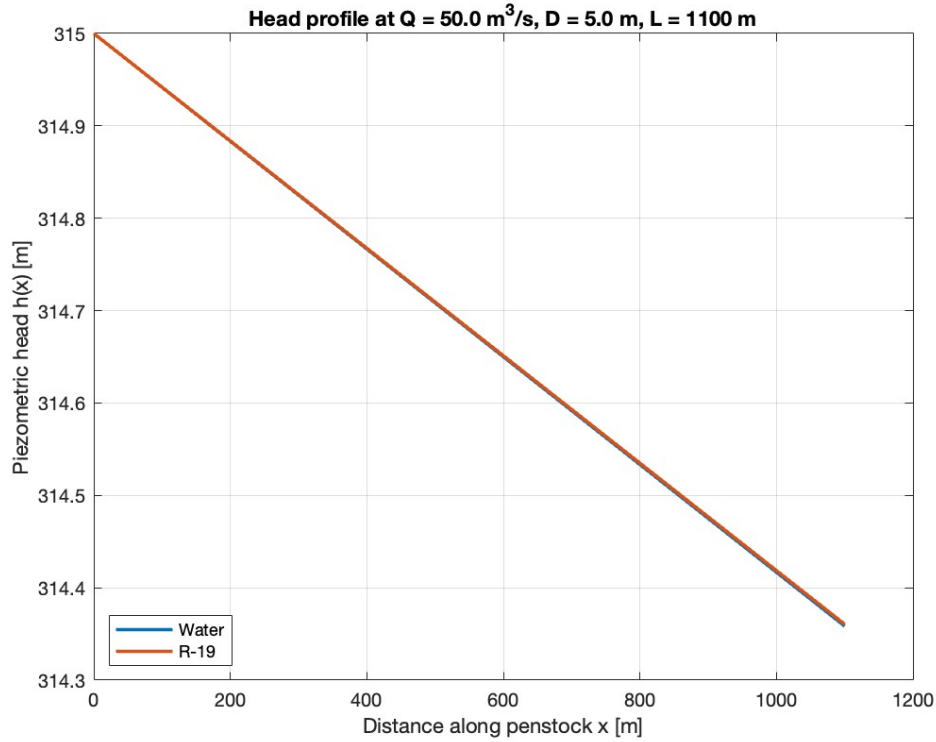


Figure 9.2: Steady-state piezometric head profile along the penstock (1100 m length) at $Q = 50 \text{ m}^3/\text{s}$ for Water vs. R-19. The head at the reservoir is about 320 m and drops by only ~ 0.6 m due to friction by the turbine inlet.

9.3 Frictional Head Loss Distribution

To examine the frictional losses in more detail, the penstock was segmented into 10 equal-length sections (each 110 m long) and the head drop across each segment was computed for water and R-19. Figure 9.3 presents a breakdown of the frictional

head loss per segment along the penstock. The blue bars show the loss Δh_f in each segment for water, and the red bars show the corresponding loss for R-19.

The segment-wise comparison highlights that the difference in frictional loss between water and R-19 is extremely small and uniformly distributed. Water incurs about 0.06414 m of loss per segment on average, while R-19 incurs about 0.06396 m per segment – a difference of only 0.00018 m per segment. In percentage terms, the total friction loss is approximately 0.204% of the available head for water, versus 0.203% for R-19. Essentially, R-19’s total friction loss is 0.289% lower than water’s.

9.4 Equivalent Head and Power for Different Fluids

A static head of $H = 320$ m of water produces a certain pressure at its base. For a denser fluid, a smaller height is sufficient to produce that same pressure. Using $H_{\text{eq}} = H \cdot \frac{\rho_{\text{water}}}{\rho_{\text{fluid}}}$, R-19 requires only about 128 m of head to exert the same pressure that water does at 320 m as seen in Figure 9.5

On the other hand, if we keep the same head as seen before, the hydraulic power potential $P_h = \rho g Q H$ scales linearly with density. At $H = 320$ m and the same Q , water provides about 157 MW per m^3/s , whereas R-19 provides about 392.4 MW – a +150% increase.

9.5 Summary Table

Table 9.3: Comparison of performance metrics for Water vs. high-density fluids at $Q = 50 \text{ m}^3/\text{s}$ and $H = 315$ m. Turbine efficiency is 90% in all cases.

Fluid	Density (kg/m^3)	Q (m^3/s)	Power (MW)	Total Head Loss (m)	Rel. Power Gain (% of H)
Water	1000	50.0	139.1	0.641	0%
R-19 Fluid	2500	50.0	347.6	0.6396	+150%

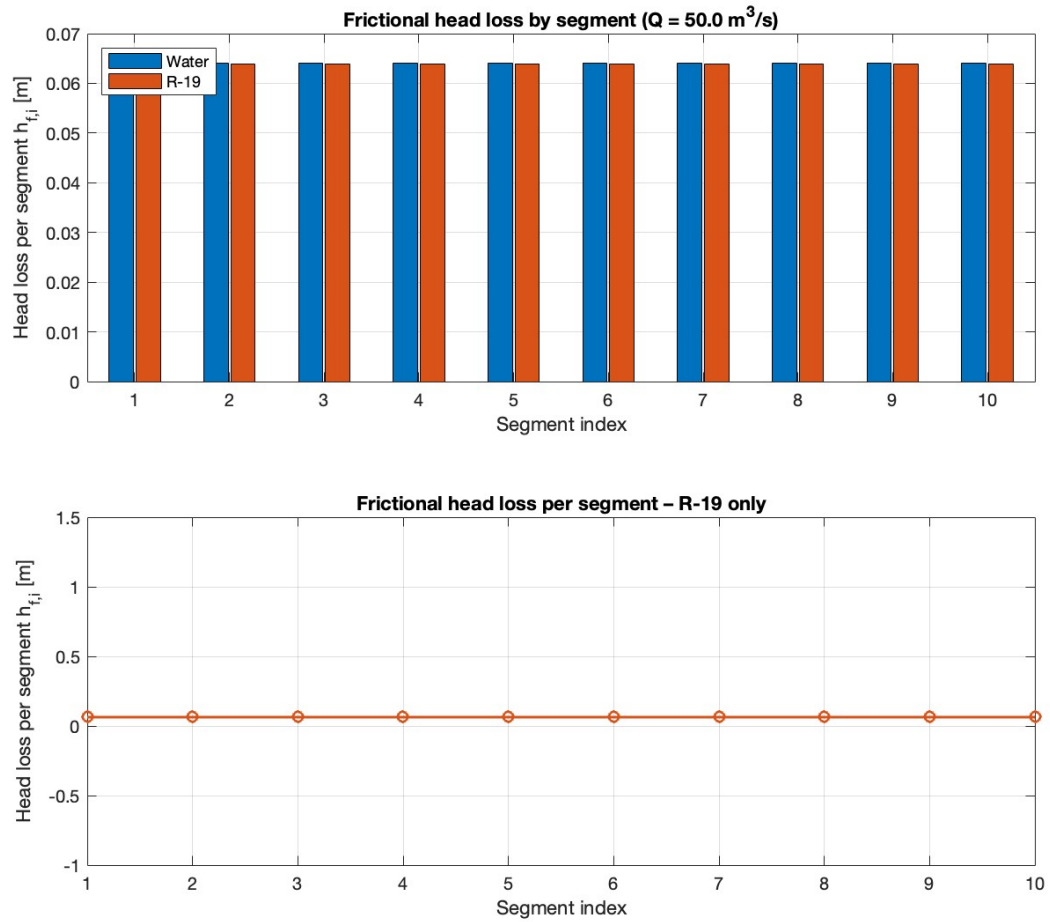


Figure 9.3: Frictional head loss per 110 m pipe segment (10 segments total) for Water vs. R-19 at $Q = 50 \text{ m}^3/\text{s}$. Losses are uniformly low along the pipe, summing to about 0.64 m over the full length.

Total Hf Water = 0.6414 m (0.204 % of H)
Total Hf R-19 = 0.6396 m (0.203 % of H)
R-19 loss is -0.289 % relative to Water

Figure 9.4: Total Frictional head loss for both fluids

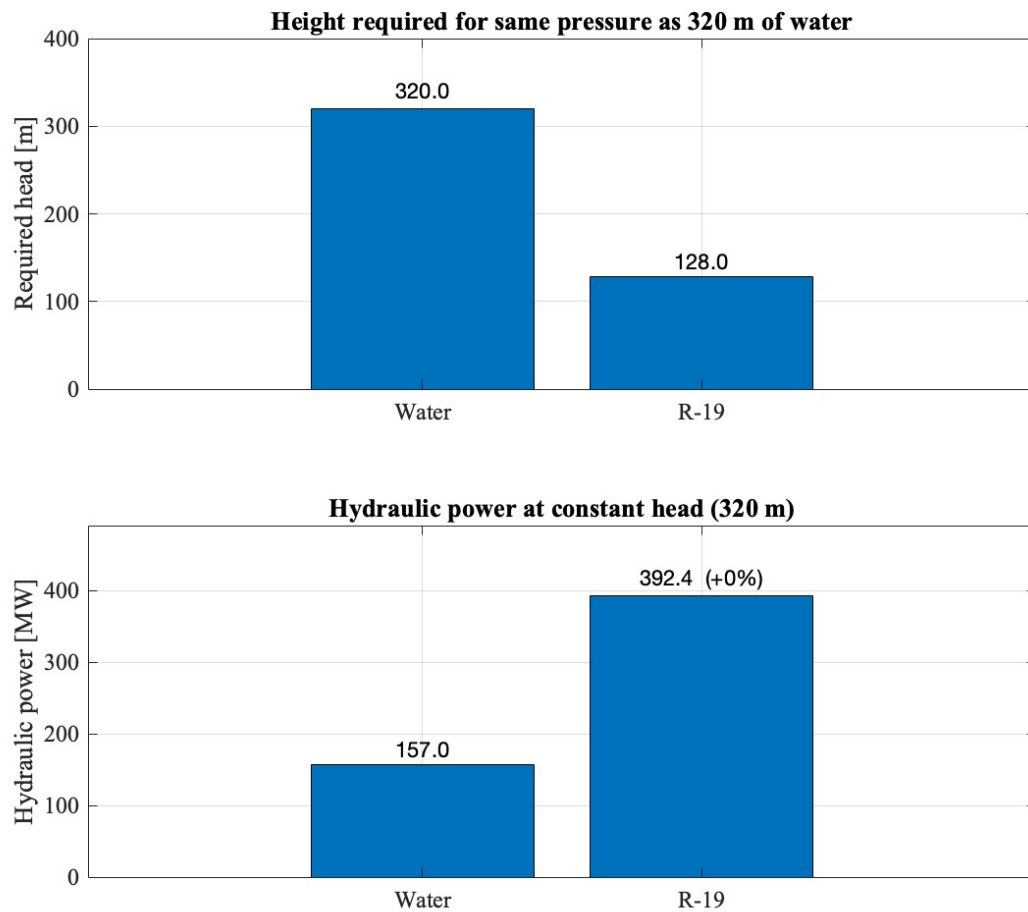


Figure 9.5: Required static head to achieve the same pressure as a 320 m water column. R-19 (density 2500 kg/m^3) produces the same pressure in only about 128 m of head.

9.6 Implications for Hydropower Repowering

The calculations show that fluid density does have an effect on the energy production of a hydropower facility, but with minimal effect on friction losses. A denser working fluid like R-19 can deliver more power from the same head and same flow conditions. The simulations showed roughly a 1.5 increase in power in going from water to a fluid 2.5 times denser, with friction losses unchanged at only 0.2% of head in both the fluids. That is practically all the additional potential energy of the high-density fluid is converted into useful work. Such performance promises to repower existing old hydropower schemes using high-density fluids, so making capacity augmentation feasible without new civil work.

Appendix A: Contribution to the United Nations Sustainable Development Goals

This project contributes directly to several of the United Nations Sustainable Development Goals (SDGs) [12]:



- **SDG 6 (Clean Water and Sanitation):** It contributes to the fulfillment of SDG 6 by making water use efficient and sustainable in the production of electricity. Generating more electricity per unit of water used results in better water-use efficiency, and retrofitting existing operating plants reduces the need for new dams, thus conserving water resources and ecosystems.



- **SDG 7 (Affordable and Clean Energy):** By maximizing the output and efficiency of hydropower plants, the project enhances SDG 7. It makes it easier to produce more renewable electricity from equal amounts of water, or even using new fluids, enabling the provision of clean, sustainable, and affordable energy for all.



- **SDG 9 (Industry, Innovation and Infrastructure):** The project achieves SDG 9 through the use of 1D hydraulic modeling and repowering

technologies in the existing HPP units. Use of a new high-density liquid (R-19) is an exemplary instance of innovation, which makes hydropower plants more productive, efficient, and durable and renovates infrastructure to make it more resilient.



- **SDG 13 (Climate Action):** It contributes to the achievement of SDG 13 by maximizing clean energy generation from hydropower. The developments reduce fossil fuel reliance and minimizes GHG emissions, raising the resilience to climate change.

Bibliography

- [1] E. Benjamin Wylie, Victor L. Streeter, and Lisheng Suo. *Fluid Transients in Systems*. ISBN 978-0-13-322173-2. Prentice Hall, 1993, p. 463. URL: <https://www.scribd.com/document/438585329/Fluid-Transients-in-Systems-Wylie-Streeter-Suo>.
- [2] J. A. Epaarachchi. *The Effect of Viscoelasticity on Fatigue Behaviour of Polymer Matrix Composites*. Ed. by R. M. Guedes. ISBN 978-0-85709-043-0. Woodhead Publishing, 2011. Chap. 17, pp. 492–513.
- [3] J. A. Epaarachchi and P. D. Clausen. *Development of a Practical Model to Predict Fatigue Life of Polymer Composites for Various Stress Ratios and Loading Frequencies*. Vol. 109. Part 2, March. International Journal of Fatigue, 2018, pp. 154–162. DOI: 10.1016/j.ijfatigue.2017.12.016. URL: <https://www.sciencedirect.com/science/article/pii/S0889974617307958>.
- [4] Christophe Nicolet. *Hydroacoustic Modelling and Numerical Simulation of Unsteady Operation of Hydroelectric Systems*. Ph.D. Thesis, Thesis No. 3751. École Polytechnique Fédérale de Lausanne (EPFL), 2007. URL: <https://infoscience.epfl.ch/record/97518>.
- [5] Stefano Cassano. *Control and Scheduling of Hybrid Hydropower Plants with Batteries for Enhanced Flexibility in Future Power Systems*. Ph.D. Thesis, NNT: 2023UPSLM041. Mines Paris – PSL / Université Paris Sciences et Lettres, 2023. URL: <https://pastel.hal.science/tel-04347682v1>.
- [6] RheEnergise Ltd. *High-Density Hydro – A New Era for Energy Storage*. Accessed: 2025-06-16. 2022. URL: <https://www.rheenergise.com/>.

- [7] Raymond Caenn, H. C. H. Darley, and George R. Gray. *Composition and Properties of Drilling and Completion Fluids*. 6th. ISBN 978-0-12-383859-9. Gulf Professional Publishing, 2011.
- [8] Robert L. Pecsok et al. *Modern Methods of Chemical Analysis*. Discusses use of CH_2I_2 as heavy liquid for density separation. John Wiley & Sons, 1976. Chap. 6.
- [9] M. Nagel and W. Köhler. *Thermal Conductivity of Galinstan and Other Liquid Metals*. Covers Galinstan properties relevant to thermal and fluid systems. Springer, 2017, pp. 55–78.
- [10] RheEnergise Ltd. *Why We Use High-Density Fluids in Energy Storage – and How We Manage Safety*. Accessed: 2025-06-16. Discusses fluid containment and environmental safety measures. 2023. URL: <https://www.rheenergise.com/technology/>.
- [11] John Twyman. *Wave Speed Calculation for Water Hammer Analysis*. No. 20, pp. 86–92. Obras y Proyectos, 2016. URL: https://www.scielo.cl/scielo.php?script=sci_arttext&pid=S0718-28132016000200086.
- [12] United Nations. *Sustainable Development Goals*. <https://sdgs.un.org/goals>. Accessed: 2025-08-13. 2015.